https://doi.org/10.5194/egusphere-2026-4864
Preprint. Discussion started: 31 August 2026

Constraining the Effects of Anthropogenic Emissions and Meteorological Variabilities on summertime $PM_{2.5}$ and surface ozone changes over eastern China during 2015-2024

Ganquan Zeng[1,2], Xiang Weng[1,2], Haofan Wang[3], Haolin Wang[4], Shuai Li[1,2], Guowen He[1,2], Ke Li[5], Meng Gao[6], Xiao Lu[1,2,*]

[1]School of Atmospheric Sciences, Sun Yat-sen University, and Southern Marine Science and Engineering Guangdong Laboratory (Zhuhai), Zhuhai, 519082, China
[2]Guangdong Provincial Observation and Research Station for Climate Environment and Air Quality Change in the Pearl River Estuary, Zhuhai, 519082, China
[3]College of Resources and Environment, Chengdu University of Information Technology, Chengdu, 610225, China
[4]School of GeoSciences, University of Edinburgh, Edinburgh, EH9 3FF, UK
[5]Jiangsu Key Laboratory of Atmospheric Environment Monitoring and Pollution Control, Collaborative Innovation Center of Atmospheric Environment and Equipment Technology, School of Environmental Science and Engineering, Nanjing University of Information Science and Technology, Nanjing, 210044, China
[6]Department of Geography, Hong Kong Baptist University, Hong Kong SAR, China

Correspondence to: Xiao Lu (luxiao25@mail.sysu.edu.cn)

Abstract.

Severe fine particulate matter ($PM_{2.5}$) and ozone pollution pose major air quality concerns in China. Chemical transport models (CTMs) are widely used to attribute their long-term trends to anthropogenic emissions and meteorological variabilities, but inherent uncertainties often yield inconsistent results across models. Here, we develop a bias correction framework that integrates a multi-layer perceptron (MLP) neural network to jointly constrain $PM_{2.5}$ and ozone attributions simulated by two independent CTMs, CMAQ and GEOS-Chem, over eastern China during 2015-2024. This framework improves simulated pollutant concentrations, spatial distributions, and interannual variabilities, providing a robust foundation for attribution analysis. During 2015-2024, anthropogenic emission changes accounted for 69-83% of the observed $PM_{2.5}$ decline and 56-63% of ozone changes across both corrected models, with meteorological variabilities contributing the remainder. Emission changes dominate the $PM_{2.5}$ decreases in 2015-2019, but the benefits weaken during 2019-2024 despite continued declines in major $PM_{2.5}$ precursors. For ozone, anthropogenic emissions drive increases during 2015-2019, but become effective for mitigating ozone thereafter. Meteorological variabilities exacerbate ozone increase in 2015-2019 but exert smaller impacts in later years. Crucially, the MLP correction reduces the inter-model attribution discrepancies from 136% to 14% for $PM_{2.5}$ and from 19% to 8% for ozone. These findings confirm the dominant role of emission changes in decadal (2015-2024) trends in summertime $PM_{2.5}$ and ozone in China, and underscore that sustained, coordinated emission reductions remain essential for mitigating both pollutants. Furthermore, they highlight the value of coupling state-of-the-art, mechanism-based CTMs with machine learning to reliably attribute long-term air quality trends.

https://doi.org/10.5194/egusphere-2026-4864
Preprint. Discussion started: 31 August 2026

1 Introduction

Fine particulate matter ($PM_{2.5}$) and surface ozone substantially affect human health and ecosystems (Burnett et al., 2018; Cohen et al., 2017; Sitch et al., 2007). Although China has witnessed a significant decline in $PM_{2.5}$ concentrations since 2013 (Zhang et al., 2019; Zheng et al., 2018), its nationwide annual concentration levels in recent years have still notably exceeded the interim target level recommended by the World Health Organization (WHO, 2021). More importantly, the rate of $PM_{2.5}$ reduction has gradually slowed in recent years (Silver et al., 2025; Geng et al., 2024), suggesting that further improvements may become increasingly difficult under lower pollution levels. In contrast, summertime ozone concentrations have not followed the same declining trend as $PM_{2.5}$ and instead exhibit persistent increases across many densely populated urban regions, such as the North China Plain and the Yangtze River Delta (Lu et al., 2020; Wang et al., 2024b). China has placed increasing emphasis on coordinated $PM_{2.5}$-ozone control, as reflected by the Air Quality Improvement Action Plan released in 2023 and the updated Ambient Air Quality Standards in 2026 (MEE, 2026).

From an atmospheric chemistry standpoint, variability in both pollutants is jointly influenced by shared precursor emissions and meteorological processes in a coupled manner. Therefore, constructing a consistent framework to simultaneously attribute their changes to anthropogenic and meteorological drivers aligns with this scientific rationale and accounts for the joint influences by both factors. Previous studies have used statistical methods, machine learning techniques, and chemical transport models (CTMs) to quantify the respective emission and meteorological effects. In short, statistical and machine learning approaches typically infer the contributions based on empirical relationships between meteorological variables and pollutant concentrations (Dai et al., 2023; Li et al., 2020; Weng et al., 2022; Zhai et al., 2019), whereas CTMs estimate these contributions by holding either emissions or meteorology constant in sensitivity simulations (Qu et al., 2025; Yang et al., 2016). Using these methods, most studies attribute $PM_{2.5}$ declines since 2013 in China primarily to anthropogenic emission reductions (Chen et al., 2020; Li et al., 2026). Attribution of ozone trends remains more uncertain, with existing studies reporting substantially different conclusions regarding the relative roles of emissions and meteorology. For example, Cao et al. (2022) identified changes in anthropogenic emissions as the predominant driver of summertime ozone increases over the North China Plain during 2012-2017, whereas Dang et al. (2021) attributed a larger contribution to meteorological variabilities (49%) than to anthropogenic emission changes (39%) over the same period. A recent study showed that the contribution of anthropogenic emission changes to the 2013-2019 summertime ozone trends in North China ranged from 45% to 86% across two chemical models and six statistical and machine learning models (Lu et al., 2025). This attribution uncertainty is further complicated by evolving emission controls and meteorological conditions, which may alter their relative roles in $PM_{2.5}$ and ozone change over time.

Discrepancies in the reported attribution outcome reflect limitations in these models. Statistical and machine learning approaches do not explicitly represent atmospheric chemistry and physics. CTMs provide process-based estimations, but their results are affected by uncertainties in emission inventories (Miao et al., 2020; Wang et al., 2021b), inaccurate representations of the chemistry (Travis and Jacob, 2019; Weng et al., 2023; Weng et al., 2026), and biased responses to changes in meteorological conditions (Li et al., 2025). These uncertainties therefore introduce systematic biases and limit their ability to reproduce observed trends (Lu et al., 2025). Recent studies have attempted to reduce these biases by

https://doi.org/10.5194/egusphere-2026-4864
Preprint. Discussion started: 31 August 2026

combining machine learning with CTMs (Liu and Xing, 2023; Ye et al., 2022; Yin et al., 2021a), but most rely on a single CTM; consequently, their attribution results remain sensitive to model-specific bias structures and cannot be evaluated across models. Most existing ML-CTM attribution studies also focus on a single pollutant, despite the strong emission and meteorological coupling effect between $PM_{2.5}$ and ozone. For example, NO_x and VOCs contribute to both photochemical ozone production and secondary aerosol formation (Shi et al., 2020; Xiao et al., 2022; Huang et al., 2021). Meteorological conditions also simultaneously affect photochemistry and accumulation and dispersion of both $PM_{2.5}$ and ozone (Jiang et al., 2022; Zhao et al., 2024). Therefore, correcting $PM_{2.5}$ and ozone separately may introduce inconsistencies in representing their coupled responses and shared sensitivities to emission and meteorological perturbations. A framework that simultaneously constrains multiple CTMs and both pollutants is therefore needed for more reliable attribution and coordinated $PM_{2.5}$-ozone control.

Here, we develop a dual-CTM, dual-pollutant bias correction framework to improve attribution of summertime (June-August) $PM_{2.5}$ and ozone changes over eastern China during 2015-2024. By integrating a data-driven dual-variate (i.e., biases in $PM_{2.5}$ and ozone) neural network, the framework simultaneously corrects both simulated pollutants. This framework is applied to the two structurally different CTMs to constrain model-dependent attribution uncertainty. This design directly addresses two key limitations in previous studies: reliance on a single pollutant- and CTM-specific correction. The bias-corrected simulations are then used to quantify the relative contributions of meteorological variabilities and anthropogenic emission changes to $PM_{2.5}$ and ozone changes, thereby reducing inter-model attribution uncertainty and providing a more reliable basis for coordinated air pollution control strategies.

2 Methods and Data

The overall attribution framework is illustrated in Figure 1. In the Step 1, we first conduct a base scenario simulation where both emissions and meteorological conditions are contemporaneous using two CTMs, the Community Multiscale Air Quality (CMAQ) and GEOS-Chem (Section 2.2). A multi-layer perceptron (MLP) neural network (Section 2.3) is then trained using biases between the observations and CTM outputs (i.e., $PM_{2.5}$ and ozone) as the two target variables whilst other simulated chemical and meteorological variables are used as input features (Section 2.4). This MLP training is conducted independently for CMAQ and GEOS-Chem. The trained MLP thereby approximates the coupled relationship mapping from CTM-simulated variables to the biases of both $PM_{2.5}$ and ozone. In the Step 2, the trained MLP models are further applied to fixed-emission scenario simulations to directly derive the bias-corrected $PM_{2.5}$ and ozone concentrations under varied meteorological conditions (i.e., bias-corrected meteorological contributions). The differences between observations and the corrected meteorologically driven variabilities thus reflect the effects of anthropogenic emissions (Section 2.5).

https://doi.org/10.5194/egusphere-2026-4864
Preprint. Discussion started: 31 August 2026

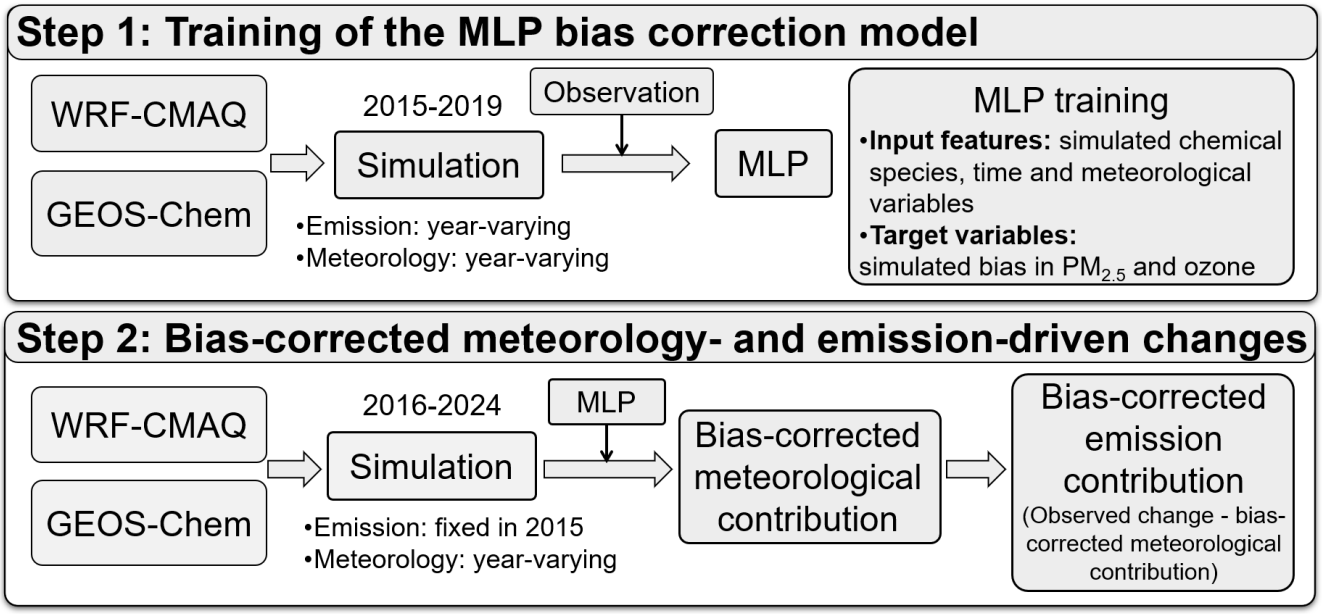

Figure 1. The workflow of dual-CTM MLP bias correction attribution framework.

2.1 Surface observation network for air pollutants and meteorological variables

This study focuses on the two densely populated city clusters in eastern China (EACN), namely, the North China Plain (NCP) and the Yangtze River Delta (YRD), with their locations and boundaries illustrated in Figure 2(b). Both regions experience severe air pollution and are regions with relatively high anthropogenic emission levels. Hourly measurements of air pollutants from the Ministry of Ecology and Environment of China and meteorological variables from the China Meteorological Administration (CMA) observations are obtained from https://quotsoft.net/air/ (X. L. Wang, 2026). Only sites with continuous records since 2015 are selected to ensure data quality and measurement continuity. Unreasonable data records, such as those exhibiting extremely large deviations from the local temporal mean or sudden hour-to-hour jumps, are discarded from analysis following Lu et al. (2018). A total of 398 sites across 84 cities are included, comprising 207 sites in 43 NCP cities and 191 sites in 41 YRD cities (Table S1).

2.2 Chemical transport models

Simulations are conducted with CMAQ and GEOS-Chem. The use of two CTMs enables a comparative evaluation of the simulated responses of $PM_{2.5}$ and ozone to anthropogenic emission changes and meteorological variabilities across eastern China. By applying a consistent bias correction to both CTMs, the machine learning framework can further reduce model uncertainties and reconcile discrepancies between the two models in quantifying meteorological and anthropogenic influences on $PM_{2.5}$ and ozone variations. The configuration details of each CTM are described below.

https://doi.org/10.5194/egusphere-2026-4864
Preprint. Discussion started: 31 August 2026

2.2.1 GEOS-Chem

We apply the global three-dimensional chemical transport model GEOS-Chem version 13.3.1 (available at https://github.com/geoschem/GCClassic/tree/13.3.1, Bey et al. (2001)). GEOS-Chem is driven by meteorological fields from the GEOS Forward Processing (GEOS-FP) which are obtained from the Goddard Earth Observing System (GEOS) of the NASA Global Modeling and Assimilation Office (GMAO). GEOS-Chem represents coupled ozone-NO_x-VOCs-aerosol-halogen tropospheric and stratospheric chemistry, and has been widely used for studies of $PM_{2.5}$ and ozone over China (e.g., Dang et al., 2021; Lu et al., 2019; Wang et al., 2021b; Xu et al., 2023).

In this study, anthropogenic emissions within China are from the Multi-resolution Emission Inventory for China (MEIC) v1.4. For regions outside China, we use the global anthropogenic emissions inventory from the Community Emissions Data System (CEDS) v_2021_04_21 (Mcduffie et al., 2020). Other natural emissions, including soil NO_x (Hudman et al., 2012; Lu et al., 2021), lightning NO_x (Murray et al., 2012), and biogenic VOC (Guenther et al., 2012), are calculated online in GEOS-Chem.

We first conduct full-year global GEOS-Chem simulations at 4° × 5° resolution for 2015-2024, using chemical initial fields from Wang et al. (2022). The resulting global fields are then used to provide initial and time-varying lateral boundary conditions for the nested-grid simulations. The nested simulations are conducted over East China (20° to 50°N, 100° to 130°E; Fig. 2) at 0.25° × 0.3125° resolution. For each nested simulation year, the model is run from 1 May to 31 August, with May used as a one-month spin-up period and June-August used for analysis. The one-month spin-up allows regional chemical fields to adjust to the nested-domain meteorology and boundary conditions before the analysis period. This spin-up length is appropriate for summertime $PM_{2.5}$ and ozone simulations over eastern China because the typical atmospheric lifetimes of these pollutants in the urban boundary layer range from hours to days (Li et al., 2025; Lu et al., 2019; Zhang et al., 2009).

The two sets of simulations are conducted, as detailed below. The first set, base simulations, are conducted with year-varying/corresponding anthropogenic emissions and meteorological conditions during June-August from 2015 to 2019. The second set of simulations covers the same months from 2016 to 2024, but with anthropogenic emissions fixed at 2015 levels while varying meteorological conditions from year to year. Simulated changes in $PM_{2.5}$ and ozone relative to 2015 therefore primarily reflect the influence of meteorological variabilities. Concentrations of key tracers are output hourly for analysis.

2.2.2 CMAQ

We use the Weather Research and Forecasting (WRFv4.2) model and the CMAQv5.5 model with a 27 km × 27 km grid resolution over a domain shown in Figure 2(a); detailed specifications are provided in Table S2. WRFv4.2 is used to simulate the meteorological fields, with initial and boundary conditions provided by NCEP (National Centers for Environmental Prediction) 1° × 1° Final (FNL) reanalysis dataset. WRF meteorological fields are evaluated against surface observations (Table S3), as shown in Figure S1 and Table S4.

The CMAQ model employs the same anthropogenic emission inventory for China (MEIC) as the GEOS-Chem model. The Carbon Bond 6 (CB06) chemical mechanism (Luecken et al., 2019) coupled with the AERO7 module (Pye et al., 2017) is adopted to model atmospheric chemistry. To reconcile differences between the MEIC emission species and the species required by the CB06 chemical mechanism, we employ the Modular Emission Inventory Allocation Tools for the Community Multiscale

https://doi.org/10.5194/egusphere-2026-4864
Preprint. Discussion started: 31 August 2026

Air Quality model (MEIAT CMAQ; https://github.com/Airwhf/MEIAT-CMAQ, last access: 15 May 2026) (Wang et al., 2024a) to assign spatial and species-specific emission data from original inventories. For the region outside of China, we adopt the MIXv2 mosaic emission inventory following Li et al. (2024c).

Consistent with the GEOS-Chem configuration, the same two sets of simulations (i.e., base and fixed-emission simulations) are also conducted in CMAQ. By adopting the same attribution experiment design and anthropogenic emission inventory for China, the CMAQ and GEOS-Chem simulations provide an opportunity to evaluate the consistency of attribution results across two independent CTMs with different representations of chemical and meteorological processes.

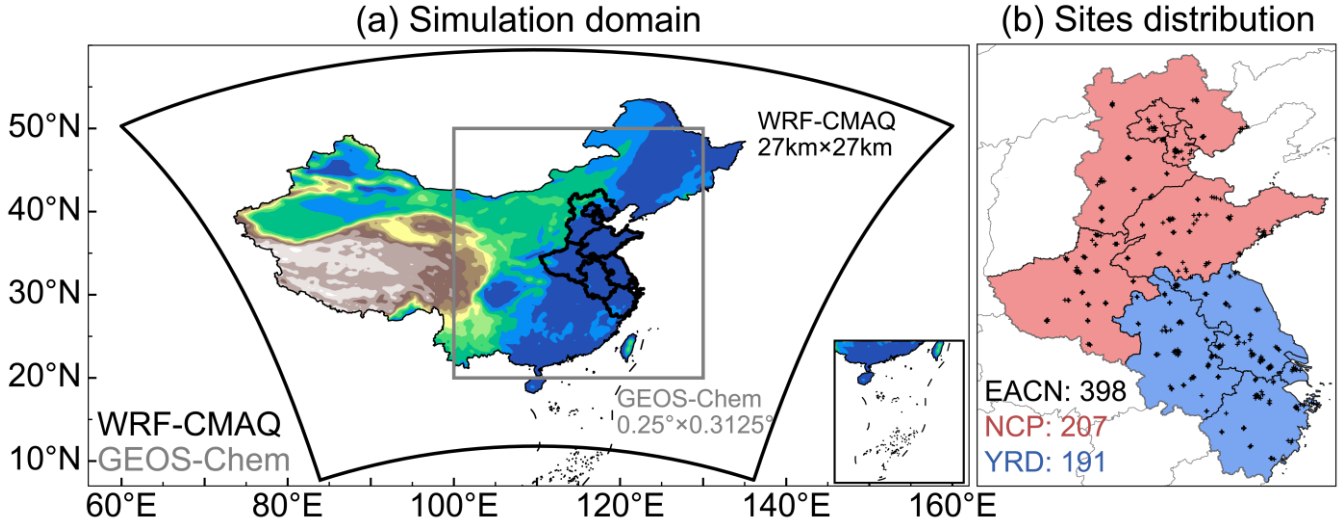

Figure 2. Modeling domains and the observational network over the study region. Panel (a) shows the simulation domains of the two models: WRF-CMAQ (black outline) and GEOS-Chem (grey rectangular outline). Panel (b) delineates the core study region, EACN, and two subregions: the area of NCP shaded in red and YRD shaded in blue. Black dots indicate the distribution of surface monitoring sites within these regions.

2.3 Multi-layer perceptron model for bias correction of simulated $PM_{2.5}$ and ozone

To correct the systematic biases of CTMs, we apply an MLP to learn the relationships between CTM-simulated variables and prediction biases of $PM_{2.5}$ and ozone, defined as the differences between simulated and observed values. This MLP-based bias correction is employed for the two CTMs, GEOS-Chem and CMAQ, in turn.

An MLP consists of an input layer, multiple hidden layers with nonlinear activation functions, and an output layer. It is trained using backpropagation to capture nonlinear relationships between input features and target variables (Gardner and Dorling, 1998; Lecun et al., 2015). In this way, the predictor variables $\boldsymbol{x} \in \mathbb{R}^{n}$ include chemical, meteorological, temporal, and geographical information, with $\boldsymbol{n}$ denoting the number of input features listed in Table 1. The output vector $\boldsymbol{y} \in \mathbb{R}^{m}$ includes the simulated bias of $PM_{2.5}$ and ozone (i.e., m= 2). $\mathbb{R}^{n}$ and $\mathbb{R}^{m}$ denote the corresponding n- and m-dimensional real-valued vector spaces, respectively. The MLP can therefore be represented as a nonlinear mapping

https://doi.org/10.5194/egusphere-2026-4864
Preprint. Discussion started: 31 August 2026

from $\boldsymbol{x}$ to $\boldsymbol{y}$, i.e., $f: \mathbb{R}^n \rightarrow \mathbb{R}^m$. By learning shared hidden representations while maintaining separate output weights for each target variable, the MLP jointly models the mapping from predictors to the multiple targets, thereby enabling simultaneous prediction of $PM_{2.5}$ and ozone biases. This joint-learning strategy helps capture the coupled responses and shared sensitivities of $PM_{2.5}$ and ozone to meteorological variabilities and atmospheric chemical processes.

The MLP uses a total of 32 (i.e., $n = 32$) input features (Table 1), including hourly chemical species from the base simulations during 2015-2019, meteorological variables from the respective driving fields (i.e., GEOS-FP for GEOS-Chem and WRF-simulated meteorology for CMAQ), cyclic temporal features (sine and cosine transformations of hour-of-day and day-of-year), and geographic features (latitude and longitude). The cyclic temporal encoding is adopted to preserve the periodic continuity of diurnal and seasonal variations, thereby allowing the MLP to better capture temporal cyclicity without introducing artificial discontinuities (Ye et al., 2026). These predictors enable the MLP to account for temporal periodicity, spatial heterogeneity and systematic biases not explicitly represented by the original CTM simulations (Keller et al., 2021; Yin et al., 2021a).

To ensure consistency between observations and model simulations, we average all observational data from monitoring sites located within the 0.25° × 0.3125° GEOS-FP grid. The biases for $PM_{2.5}$ and ozone are then calculated on a grid-by-grid basis. For GEOS-Chem, simulated concentrations are directly available at the target resolution. For WRF-CMAQ (27 km × 27 km, Lambert conformal projection), CMAQ outputs are remapped onto the 0.25° × 0.3125° GEOS-Chem grid using nearest-grid interpolation based on CMAQ grid centers. Because the horizontal resolutions of the two models are comparable, this remapping introduces only minor spatial representativeness differences while allowing direct comparison between the two CTMs and observations within a unified framework. After spatial matching, 139 grid cells with observational constraints are used to train the MLP for the two CTMs in turn. All samples from these grids are subsequently combined into a unified training dataset. Compared with training independent models for individual grid cells, this unified strategy enables the model to learn shared spatiotemporal relationships across regions and to exploit common patterns among grids with similar meteorological and emission characteristics, thereby improving model robustness within the observed monitoring domain. The training, cross-validation, and application procedures are described in section 2.4.

2.4 Training, cross-validation, and application of the MLP model

Using the dataset described in Sect. 2.3, we train a fully connected feedforward MLP and optimize three hyperparameters: the hidden-layer configuration, learning rate, and batch size. The input and output dimensions are fixed at 32 and 2, representing the 32 input features and the two target biases for $PM_{2.5}$ and ozone, respectively. We test three configurations of four hidden layers: [2048, 1024, 512, 256], [1024, 512, 256, 128], and [512, 256, 128, 64], where values in brackets denote the numbers of neurons in the four hidden layers, respectively. Candidate learning rates are 0.01 and 0.001, and candidate batch sizes are 512, 1024, and 2048. Batch size denotes the number of training samples processed before each update of the model weights and is not part of the network architecture.

We focus only on the model grid cells for which observations are available. To train the MLP, we use all the gridded hourly data from the study domain, rather than training a separate model for each grid cell. Each gridded hourly record from a particular grid cell is treated as a sample containing the 32 input features and the two target biases, i.e., the differences between the observed and modeled $PM_{2.5}$ and ozone

https://doi.org/10.5194/egusphere-2026-4864
Preprint. Discussion started: 31 August 2026

concentrations, respectively, as defined in Sect. 2.3. Before data splitting, the hourly samples from all grid cells with valid observations are combined into one dataset. Latitude and longitude are included among the 32 input features so that the MLP can account for geographic differences in the target biases and in their relationships with the other input features.

For tuning and evaluating the MLP, we use five-fold cross-validation with a date-based temporal rotation. Specifically, all unique calendar dates represented in the gridded hourly data from the study domain are randomly assigned to five folds. The samples remain at their original hourly resolution and are not averaged into daily values. Instead, each date and all the hourly samples from that date are kept together and assigned to the same fold. In each iterative run of five-fold cross-validation, one date fold is held out as the test set, while the remaining four date folds form the model-development dataset. Within this dataset, a similar five-fold splitting process is conducted for hyperparameter tuning: one fold is held out as the validation set, while the remaining four folds are used for model training.

Within a run, all hourly samples from a given date, including those from different hours and grid cells, are assigned to the same set. Thus, no date occurs in more than one of the training, validation, and test sets, preventing samples from the same day from being used in both model development and evaluation. The training set is used for model fitting, the validation set is used for hyperparameter selection and early stopping, and the final model is applied to the test fold held out at the beginning of the run. Because the data are split by date rather than grid cell, this procedure evaluates the model on excluded dates at locations with observations, rather than at locations without observations. For each run, the means and standard deviations used to standardize the input features are calculated from the training set only and then applied unchanged to the corresponding validation and test sets.

Hyperparameters are selected separately within each run. For every candidate combination of hidden-layer configuration, learning rate, and batch size, an MLP is trained on the training set for 20 epochs and evaluated on the corresponding validation set using mean squared error (MSE). The combination producing the lowest validation MSE is selected for that run. The models trained for 20 epochs are used only to compare the candidate combinations and are not used for test prediction. An MLP using the selected hidden-layer configuration, learning rate, and batch size is then trained on the same training set for up to 300 epochs. During this training, the model weights from the epoch with the lowest validation MSE are retained, and training is stopped if the validation MSE does not improve for 30 consecutive epochs. The retained model is then used to predict the test fold, which is not used for hyperparameter selection, model fitting, or early stopping.

Across the five runs, each date fold serves as the test set once. The predictions from the five test folds are then combined. Because each test prediction is generated by a model trained without the corresponding date, these combined results are referred to as out-of-fold predictions and are used to calculate the overall cross-validation performance.

Table 1. Feature variables used in MLP model.

Variable	GEOS-Chem	WRF-CMAQ
Chemical species variables		
Carbon monoxide	CO	
Dinitrogen pentoxide	N2O5	
Ammonia	NH3	
Nitric oxide	NO	

https://doi.org/10.5194/egusphere-2026-4864
Preprint. Discussion started: 31 August 2026

Nitrogen dioxide	NO2	
Hydroxyl radical	OH	
Sulfur dioxide	SO2	
Peroxyacetyl nitrate	PAN	
Ozone	O3	
Fine particulate matter	PM2.5	
Volatile organic compounds (non-methane hydrocarbons, aldehydes, and ketones, etc.)	VOCs	
Black carbon	BC	PMF_EC
Ammonium	NH4	ANH4J
Inorganic nitrate	NIT	ANO3J
Organic carbon	OC	PMF_POA
Secondary organic aerosol	SOA	PMF_SOA
Ratio of black carbon and organic carbon	BC_OC_ratio	EC_POA_ratio
Meteorological variables		
Planetary boundary layer height	PBLH	
Relative humidity	RH	
Sea level pressure	SLP	
temperature	T2	
Zonal wind at 10 m	U10M	
Meridional wind at 10 m	V10M	
Total precipitation	PRECTOT	RAIN
Solar radiation	SWGDN	SWDOWN
Geographic information		
Longitude	lon	
Latitude	lat	
Time information		
Hour of the day	Hour	
Sine-transformed hour-of-day	hour_sin	
Cosine-transformed hour-of-day	hour_cos	
Sine-transformed day-of-year	doy_sin	
Cosine-transformed day-of-year	doy_cos	

2.5 Attribution of $PM_{2.5}$ and ozone change to emission and meteorology

The trained MLP models predict the biases of the CTMs relative to observations. Consequently, the MLP-corrected results (obtained by adding the predicted biases to the original CTM simulations) are expected to closely match the observations, as will be demonstrated in Section 3. Although this approach does not directly modify the model inputs (e.g., meteorological fields or emission inventories) or internal mechanisms, it effectively constrains the CTMs to capture the observed temporal changes in $PM_{2.5}$ and ozone, a critical prerequisite for the accurate attribution of their variability. To isolate the meteorological impacts, we apply this MLP-based correction to sensitivity simulations from both CTMs spanning 2016 to 2024, in which anthropogenic emissions are fixed at 2015 levels while meteorological conditions are allowed to vary (Section 2.2). The MLP-corrected results thus represent an improved prediction of $PM_{2.5}$ and ozone levels that would occur under the meteorology of a given year, assuming anthropogenic emissions remain fixed at the 2015 levels. In other words, these results represent the variability in $PM_{2.5}$

https://doi.org/10.5194/egusphere-2026-4864
Preprint. Discussion started: 31 August 2026

and ozone concentrations solely driven by changes in meteorological variabilities. These bias-corrected fixed-emission simulations are denoted as $MLP_{\text{year}}^{\text{CTM}}$, where the subscript $year$ refers to individual years from 2016 to 2024. The meteorology-driven change relative to 2015 (ΔMet) for either $PM_{2.5}$ or ozone is defined as:

$$\Delta\text{Met}_{\text{year}} = MLP_{\text{year}}^{\text{CTM}} - MLP_{2015}^{\text{CTM}} \quad (1)$$

Evidently, the year-to-year observed change is defined as:

$$\Delta\text{Obs}_{\text{year}} = \text{Obs}_{\text{year}} - \text{Obs}_{2015} \quad (2)$$

Following previous studies (Keller et al., 2021; Yin et al., 2021a), we assign the residuals derived from the subtraction between observed changes and bias-corrected meteorologically driven changes as the emission-driven component:

$$\Delta\text{Obs}_{\text{year}} = \Delta\text{Emis}_{\text{year}} + \Delta\text{Met}_{\text{year}} \quad (3)$$

Using this framework, we can quantify the relative contributions of emission changes and meteorological variabilities to interannual variations in $PM_{2.5}$ and ozone during 2016-2024. Compared to traditional CTM-based attribution that directly relies on simulations with fixed meteorology or emissions, a key advantage of applying this approach is that it accounts for systematic biases in CTM predictions of $PM_{2.5}$ and ozone. This allows for more accurate concentration estimates under varying meteorological scenarios, thereby better isolating the contributions of meteorology (Equation 1) and thus emissions (Equation 3) to the observed interannual variability of these pollutants. Furthermore, the use of two CTMs enables cross-model comparison and helps assess uncertainties associated with differences in model structures and process representations.

3 Evaluation of MLP-corrected CTM simulations

Although both CMAQ and GEOS-Chem generally reproduce the temporal variations and spatial patterns of summertime $PM_{2.5}$ and MDA8 ozone over eastern China during 2015-2019, they retain substantial biases, as shown in Figures 3 and 4. Overall, CMAQ shows relatively better agreement with observations for both $PM_{2.5}$ and ozone, with consistently lower simulation biases than GEOS-Chem. For $PM_{2.5}$, GEOS-Chem exhibits persistent and large high biases compared to observations, yielding a root-mean-square error (RMSE) of 23.7 μg m^{-3} (Fig. 3b). Previous studies similarly reported systematic $PM_{2.5}$ overestimations in GEOS-Chem over eastern China, indicating potential uncertainties in nitrate deposition and oversimplified secondary organic aerosol formation (e.g., Xu et al., 2023; Miao et al., 2020). For ozone, both models here generally overestimate summertime concentrations throughout the study period (Figs. 3c and 3d), although the overall biases are smaller in CMAQ (RMSE = 12.9 ppb) than in GEOS-Chem (RMSE = 20.3 ppb). Similar overestimations were reported in previous CTM studies over eastern China and were partly attributed to uncertainties in aerosol-related chemical processes and emission inventories (e.g., Gao et al., 2024; Hou et al., 2022; Sun et al., 2026).

We evaluate the performance of MLP-based bias correction using held-out testing data and the five-fold cross-validation approach described in Sect. 2.4. Predictions from the test fold in each cross-validation round are concatenated to evaluate the bias-corrected results over the full 2015-2019 training period. Hereafter, the MLP-corrected CMAQ and GEOS-Chem simulations (i.e., adding the MLP-predicted biases to the original CTM prediction results) are denoted as CMAQ-MLP and GC-MLP,

https://doi.org/10.5194/egusphere-2026-4864
Preprint. Discussion started: 31 August 2026

respectively. Based on these testing data, the RMSE values of $PM_{2.5}$ during 2015-2019 decrease from 9.6 to 5.2 μg m^{-3} for CMAQ-MLP and from 23.7 to 4.1 μg m^{-3} for GC-MLP (Figs. 3a and b). Meanwhile, the RMSEs of MDA8 ozone decrease from 12.9 to 6.2 ppb in CMAQ-MLP and from 20.3 to 3.8 ppb in GC-MLP (Fig. 3c and d). The spatial distributions of both pollutants are also improved after bias correction (Fig. 4), particularly for CMAQ, with the spatial Pearson correlation coefficients of $PM_{2.5}$ and ozone increasing from 0.23 and 0.46 to 0.97 and 0.96, respectively. This underscores the generalizability of the MLP bias correction method between these two CTMs, which is noteworthy given that both models may contain vastly different structural biases as evidenced by their large disagreement in simulated $PM_{2.5}$ and ozone levels and variabilities.

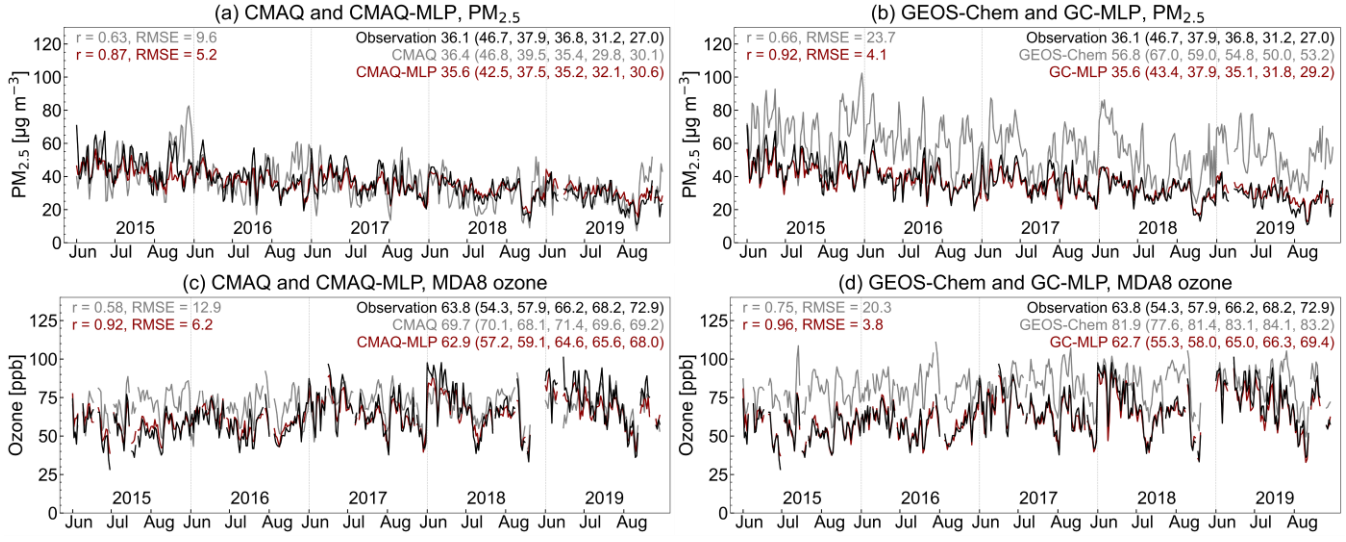

Figure 3. Temporal variations of observed and simulated summer $PM_{2.5}$ and MDA8 ozone during 2015-2019 from CMAQ, GEOS-Chem, and their MLP-corrected simulations. The MLP-corrected results are evaluated using held-out testing data from the day-based five-fold cross-validation, with predictions from each test fold concatenated to cover the full 2015-2019 period. The black solid lines represent ground-based observations, while the grey and red solid lines denote the original CTMs (CMAQ or GEOS-Chem) and the bias-corrected models (CMAQ-MLP or GC-MLP), respectively. Correlation coefficients (r) and RMSE between simulated and observed values are shown inset. The five-year and individual annual mean values are shown in the upper right of each panel, outside and inside parentheses, respectively.

https://doi.org/10.5194/egusphere-2026-4864
Preprint. Discussion started: 31 August 2026

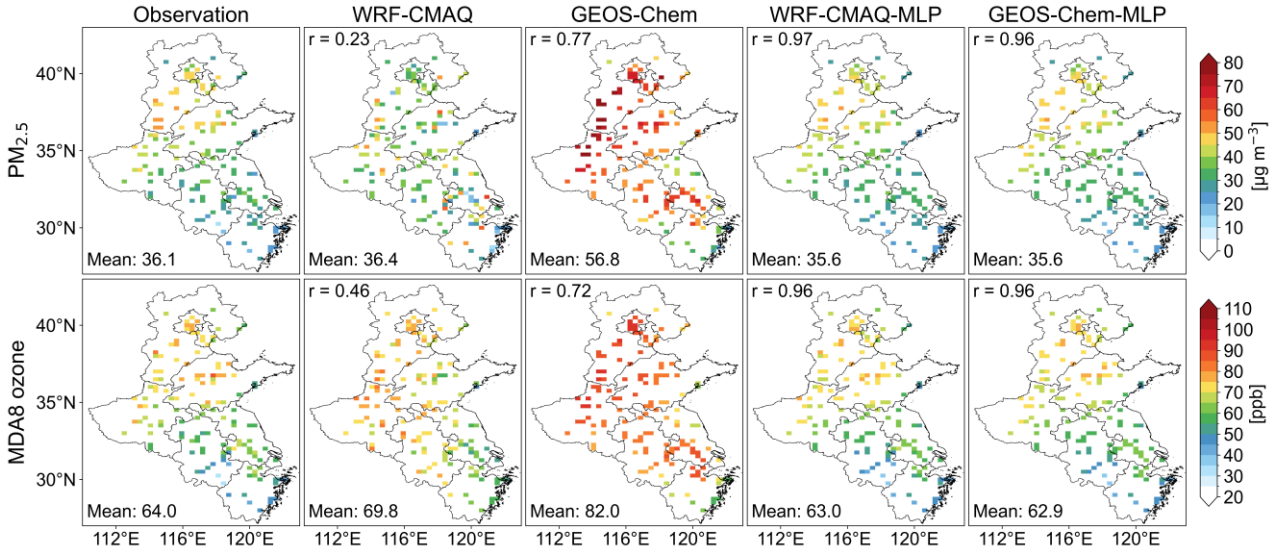

Figure 4. Spatial distributions of summertime daily $PM_{2.5}$ (top row) and MDA8 ozone (bottom row) during 2015-2019 from observations, CMAQ, GEOS-Chem, CMAQ-MLP, and GC-MLP. Mean concentrations and spatial correlation coefficients (r) between simulated and observed values are shown inset.

The enhanced representation of observed interannual trends by the MLP-based correction is particularly notable. For ozone, observations show a substantial increase of 4.8 ppb $year^{-1}$ over the EACN region during the 2015-2019 training period. In comparison, CMAQ simulates flat or even negative ozone trends across these regions (-0.2 to 0.2 ppb $year^{-1}$), while GEOS-Chem reproduces only weak positive trends (1.2 to 1.6 ppb $year^{-1}$) (Fig. 5d). This discrepancy is evident in both the NCP and YRD regions (Fig. 5e-f), indicating that both CTMs struggle to capture ozone responses to interannual variations in emissions (from the MEIC inventory) and meteorology, as previously reported (e.g., Lu et al., 2025). Following the MLP-based correction, the ozone trends reach 2.8 and 3.7 ppb $year^{-1}$ for CMAQ-MLP and GC-MLP over the EACN region, respectively, aligning much more closely with the observations. For $PM_{2.5}$, the corrected simulations still capture the observed declining trends with much improved performance on absolute values (Fig. 5a-c). Importantly, this improved trend representation is achieved without compromising the spatial and temporal consistency of pollutant distributions (Fig. 4). This capability is particularly vital for studies focusing on long-term air quality trends, where accurately reproducing interannual trends is more critical than merely improving mean-state statistical performance.

https://doi.org/10.5194/egusphere-2026-4864
Preprint. Discussion started: 31 August 2026

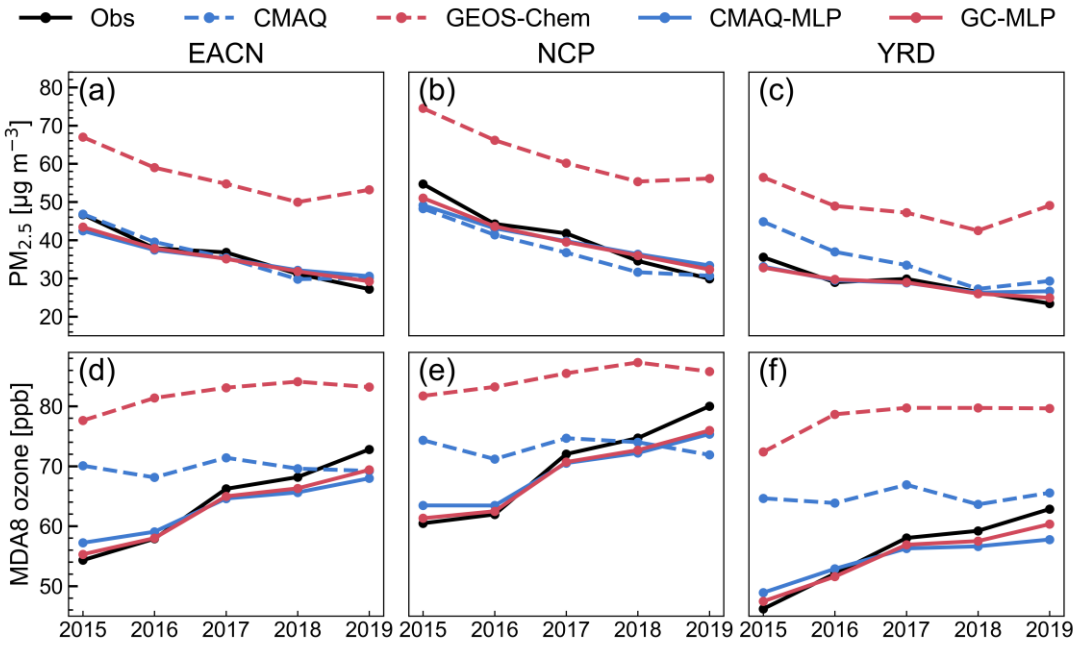

Figure 5. Time series of observed, CMAQ, GEOS-Chem, and their MLP-corrected simulations of $PM_{2.5}$ and MDA8 ozone across EACN, NCP, and YRD. The top panels (a-c) show the annual variations of $PM_{2.5}$, and the bottom panels (d-f) present those of MDA8 ozone from 2015 to 2019. Columns from left to right represent the three target regions: EACN, NCP, and YRD. The black line with solid circles denotes the ground-based observations (Obs). Dashed lines denote the original CTM simulations from CMAQ (blue) and GEOS-Chem (red). Solid lines denote the corresponding bias-corrected models (CMAQ-MLP in blue and GC-MLP in red).

4 Attribution of 2015-2024 $PM_{2.5}$ and ozone change in eastern China

4.1 2015-2024 trends and attributions

Section 3 demonstrates that the MLP-based correction method successfully mitigates the spatiotemporal biases of summertime $PM_{2.5}$ and ozone in both CTMs in 2015-2019 when evaluated on held-out test data. We now rely on this approach to further attribute the 2015-2024 $PM_{2.5}$ and ozone trends to anthropogenic emissions and meteorology as described in Section 2.5. Here, we apply a "final" MLP-based correction trained on the entire 2015-2019 dataset, utilizing the optimal hyperparameters identified through the day-based five-fold cross-validation. This strategy maximizes data utilization to achieve the best fit to observations, thereby yielding more robust estimates for the attribution compared with results derived from held-out test data.

During 2015-2024, observed summertime $PM_{2.5}$ concentrations over eastern China decrease at a rate of -2.9 μg m^{-3} $year^{-1}$ (Fig. 6a). Both CMAQ-MLP and GC-MLP attribute most of this decline to anthropogenic emission reductions, with smaller contributions from meteorological variabilities. In CMAQ-MLP, emission changes contribute -2.4 μg m^{-3} $year^{-1}$, accounting for about 83% of the observed $PM_{2.5}$ decline, while meteorological variabilities contribute -0.5 μg m^{-3} $year^{-1}$. In GC-MLP, emission changes contribute -2.0 μg m^{-3} $year^{-1}$, corresponding to about 69% of the observed decline, while

https://doi.org/10.5194/egusphere-2026-4864
Preprint. Discussion started: 31 August 2026

meteorological variabilities contribute -0.9 μg m^{-3} $year^{-1}$. These results indicate that CMAQ-MLP and GC-MLP agree that emission changes are the dominant driver of the observed decadal decline in summertime $PM_{2.5}$ over eastern China.

For MDA8 ozone, observations show an increasing trend of 1.3 ppb $year^{-1}$ during 2015-2024 (Fig. 6b). Trend decompositions from both MLP-corrected models consistently identify anthropogenic emissions as the primary driver. CMAQ-MLP estimates that emission changes drive 69% (0.9 ppb $year^{-1}$) of this surge, outweighing the meteorological contribution of 31% (0.4 ppb $year^{-1}$). While GC-MLP suggests a stronger secondary role for meteorology (0.6 ppb $year^{-1}$, or 46%), it still identifies emissions as the leading factor, responsible for the remaining 54% (0.7 ppb $year^{-1}$) of the long-term trend.

Notably, both corrected models reveal that the relative contributions of emissions and meteorology vary substantially over time throughout 2015-2024. To examine these temporal differences, the study period is further divided into two sub-periods (2015-2019 and 2019-2024) in Sections 4.2 and 4.3. The year 2019 is selected as the transition point because anthropogenic emissions underwent more abrupt changes after 2020 due to the COVID-19 lockdown (Huang et al., 2021; Le et al., 2020; Yin et al., 2021b). We separately discuss the relative role of emission changes and meteorological variabilities in Section 4.2 and Section 4.3.

https://doi.org/10.5194/egusphere-2026-4864
Preprint. Discussion started: 31 August 2026

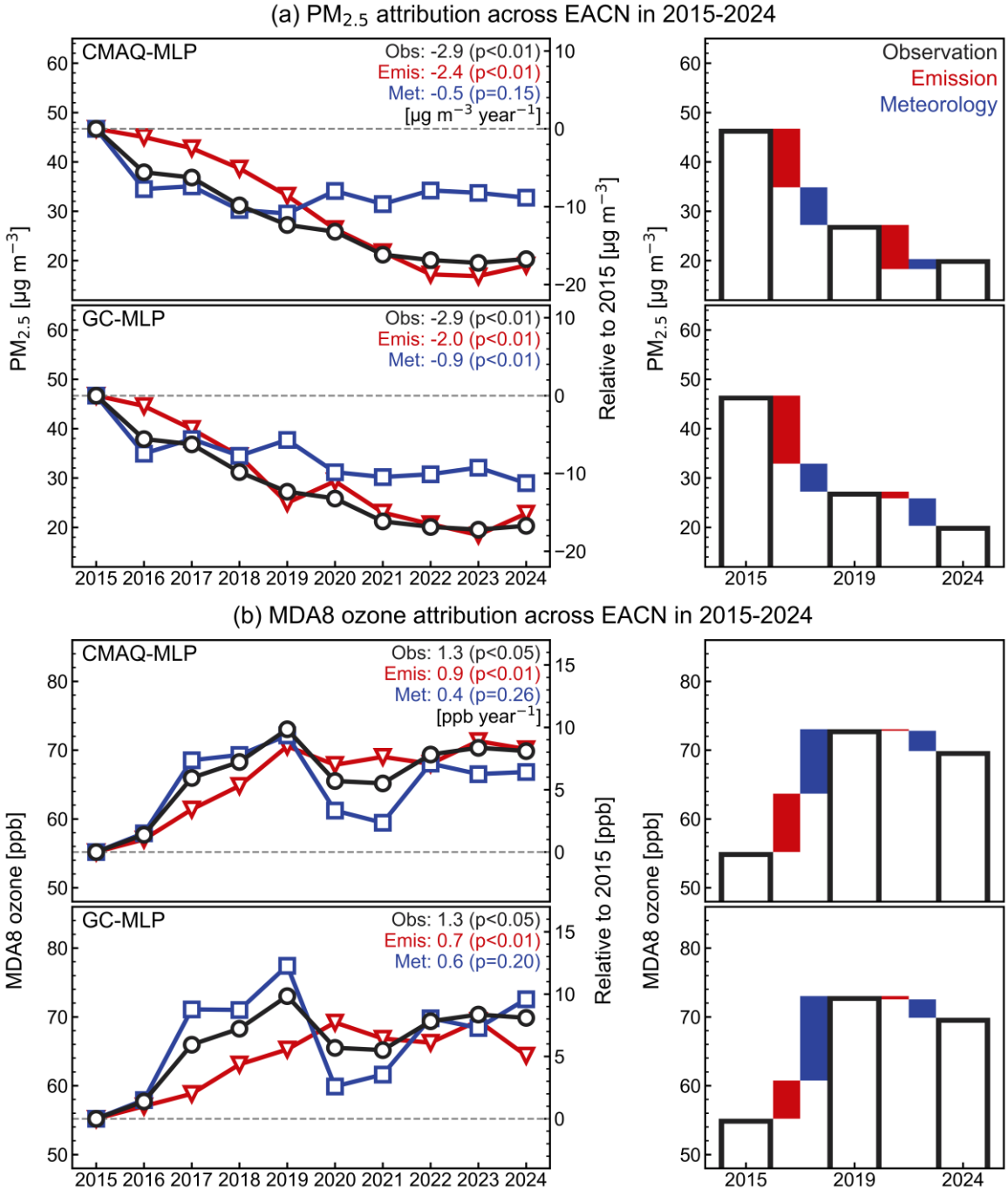

Figure 6. Attribution of changes in (a) $PM_{2.5}$ and (b) MDA8 ozone concentrations to emission reductions and meteorological variabilities over eastern China during 2015-2024. Left panels show the time series of observed concentrations (black lines with circles), and the contributions from emission changes (red lines with triangles) and meteorological variabilities (blue lines with squares) derived from the CMAQ-MLP and GC-MLP bias-corrected models. Right panels illustrate the attribution results for different periods, showing concentration changes in 2019 relative to 2015 and in 2024 relative to 2019, highlighting the respective roles of emission changes and meteorological variabilities during different stages of air-quality evolution.

https://doi.org/10.5194/egusphere-2026-4864
Preprint. Discussion started: 31 August 2026

4.2 Emission-driven changes in $PM_{2.5}$ and ozone

Anthropogenic emissions over EACN decrease substantially during 2015-2023, with cumulative reductions ranging from 20% for VOCs to 66% for SO_2 relative to the 2015 level (Fig. S2), according to the MEIC v2.0 emission inventory used in the simulation. The temporal evolution of emissions broadly reflects China's clean-air policies. The 2015-2019 period covers the latter part of the Air Pollution Prevention and Control Action Plan (2013-2017) and the initial implementation of the Three-Year Action Plan for Winning the Blue Sky Defense Battle (2018-2020), which emphasizes $PM_{2.5}$ reduction through controls on coal combustion and industrial sources. Consistent with these priorities, emission reductions over EACN during 2015-2019 are larger for SO_2 (51%), primary $PM_{2.5}$ (32%), and CO (26%) than for NO_x (18%) and VOCs (8%). After 2019, particularly during the 14th Five-Year Plan period (2021-2025), air-pollution control increasingly emphasizes coordinated $PM_{2.5}$-ozone mitigation and joint reductions in VOC and NO_x emissions. Correspondingly, VOC emission reductions increase from 8% during 2015-2019 to 13% during 2019-2023, while NO_x emission reductions remain steady (17%).

Dynamic shifts in these primary anthropogenic emissions act as the key modulator for the observed temporal trends in both $PM_{2.5}$ and ozone. During 2015-2019, both CMAQ-MLP and GC-MLP attribute the observed $PM_{2.5}$ (-4.5 μg m^{-3} $year^{-1}$ over EACN) decline primarily to anthropogenic emission reductions, with emission-driven trends of -2.9 (64% of observed trend) and -3.4 (76%) μg m^{-3} $year^{-1}$, respectively (Figs. 7a1 and b1). This attribution is supported by concurrent decreases in observed NO_2 (14%) and SO_2 (51%) concentrations (Fig. 8). Both bias-corrected models further show spatially widespread emission-driven $PM_{2.5}$ decreases, with the strongest responses over the NCP (CMAQ-MLP: 3.7; GC-MLP: 4.5 μg m^{-3} $year^{-1}$), substantially exceeding those in the YRD (1.7 and 1.9 μg m^{-3} $year^{-1}$). These emission-driven $PM_{2.5}$ decreases account for 63-76% and 63-72% of the observed $PM_{2.5}$ decreases in NCP and YRD, respectively. The stronger response in the NCP is consistent with larger decreases in observed NO_2 and SO_2 concentrations than in the YRD. The agreement between both models indicates that the dominant role of emission reductions in the $PM_{2.5}$ decrease during this period is robust. More importantly, the regional contrast suggests that larger precursor reductions are associated with greater $PM_{2.5}$ benefits, highlighting the effectiveness of stringent emission controls during the relatively polluted early stage of the study period.

https://doi.org/10.5194/egusphere-2026-4864
Preprint. Discussion started: 31 August 2026

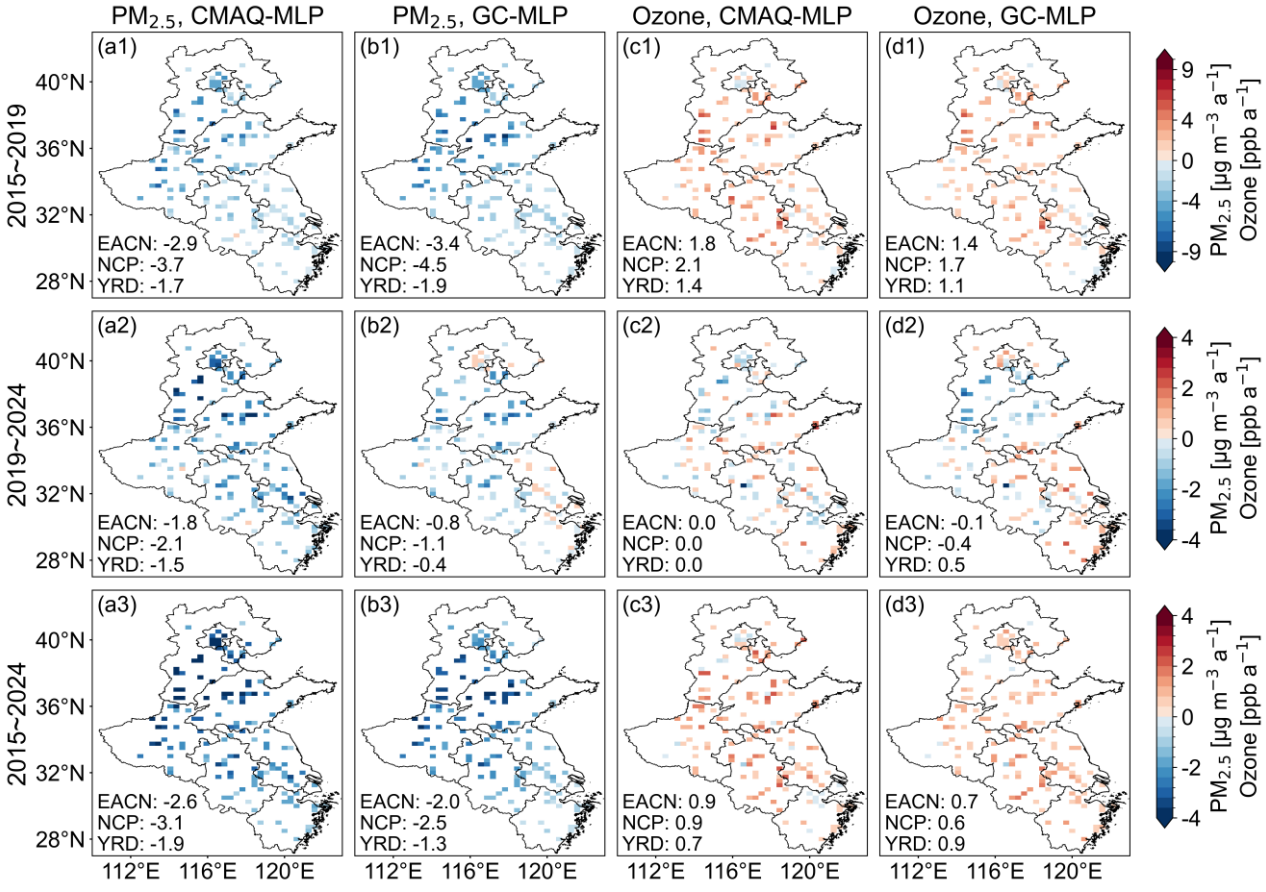

Figure 7. Spatial distribution of anthropogenic emission-driven changes in summertime surface daily $PM_{2.5}$ and ozone concentrations over eastern China during three analysis periods (2015-2019, 2019-2024, and the overall 2015-2024 period) as attributed by CMAQ-MLP and GC-MLP. Panels (a, b) show the emission-driven contributions to $PM_{2.5}$ changes derived from CMAQ-MLP and GC-MLP, respectively. Panels (c, d) show the same but for ozone. Trends at each grid cell are calculated based on monthly mean daily $PM_{2.5}$ and MDA8 ozone concentration anomalies defined as the deviation of the monthly mean from the multi-year average of the corresponding calendar month over 2015-2024.

After 2019, emission reductions continue to lower $PM_{2.5}$, but the magnitude of the response weakens sharply in both corrected models (Figs. 7a2 and b2). Over the NCP, the emission-driven decrease falls from 3.7-4.5 μg m^{-3} $year^{-1}$ during 2015-2019 to 1.1-2.1 μg m^{-3} $year^{-1}$ during 2019-2024; over the YRD, it falls from 1.7-1.9 to 0.4-1.5 μg m^{-3} $year^{-1}$. Notably, the weaker emission-driven $PM_{2.5}$ decrease during 2019-2024 is not accompanied by a comparable slowdown in reductions of precursor concentrations. During 2019-2024, observed NO_2 concentrations exhibit accelerated declines of 38% in the NCP and 29% in the YRD, surpassing the reductions seen in 2015-2019 (15% and 12%, respectively). This accelerated urban NO_2 decline reflects a shift in NO_x mitigation strategies, transitioning from early reductions driven largely by power-sector controls to increasingly stringent regulations on industrial and urban transport sources after 2020 (Li et al., 2024a; Zheng et al., 2018). By contrast, SO_2 reductions decelerate from 53% to 34% in the NCP and from 46% to 12% in the YRD (Fig. 8). Together, these results indicate that the

https://doi.org/10.5194/egusphere-2026-4864
Preprint. Discussion started: 31 August 2026

$PM_{2.5}$ response does not scale directly with the magnitude of observed precursor decreases after 2019, pointing to a possible decrease in the marginal $PM_{2.5}$ benefits of additional precursor controls under cleaner atmospheric conditions (Dao et al., 2026; Li et al., 2023). The stronger emission-driven $PM_{2.5}$ decreases in the NCP than in the YRD during 2019-2024 further indicate that $PM_{2.5}$ responses to continued precursor reductions vary across atmospheric chemical environments.

The difference in emission-driven $PM_{2.5}$ responses between the NCP and YRD may partly reflect contrasts in sulfate-nitrate-ammonium (SNA) chemistry and ammonia availability. Previous studies have shown that the NCP is characterized by substantially higher atmospheric ammonia levels (e.g., Liu et al., 2018; Sun et al., 2025; Zhang et al., 2018), resulting in abundant ammonium availability for SNA formation and stronger interactions among sulfate, nitrate, and ammonium components (Wang et al., 2013; Pinder et al., 2007). In the ammonia-rich NCP, available ammonia continues to support nitrate partitioning, maintaining a strong potential for $PM_{2.5}$ reductions in response to ongoing NO_x and SO_2 controls after 2019. In contrast, limited ammonia in YRD renders $PM_{2.5}$ insensitive to NO_x reductions, while the diminishing rate of SO_2 decline further restricts the decrease in $PM_{2.5}$ concentrations. This interpretation is broadly consistent with previous analyses (e.g., Chen et al., 2016; Geng et al., 2017), which show that regional ammonia availability can regulate the sensitivity of $PM_{2.5}$ to precursor reductions through thermodynamic partitioning within the SNA system. It also highlights the critical need to control ammonia emissions to effectively mitigate $PM_{2.5}$ pollution (Gu et al., 2021; Zhai et al., 2021). Furthermore, observational evidence since 2013 has demonstrated smaller reductions in secondary organic aerosols (SOA) compared to primary organic aerosols (Chen et al., 2024). The complex effects of reducing NO_x and SO_2 on SOA production may have even led to slight overall increases in SOA (Chen et al., 2024), indicating that SOA formation chemistry could complicate the response of $PM_{2.5}$ to further NO_x and SO_2 reductions.

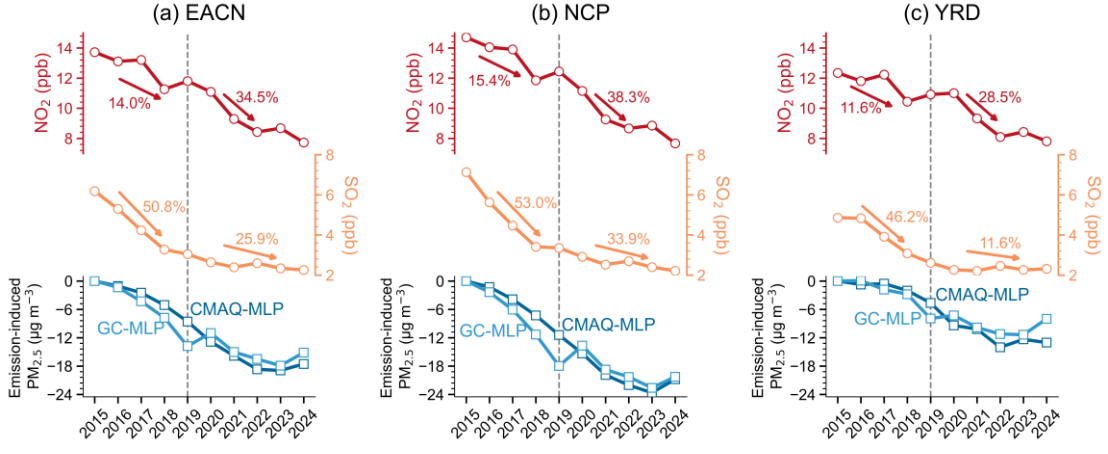

Figure 8. Observed NO_2 and SO_2 concentrations and emission-induced $PM_{2.5}$ changes provided by CMAQ-MLP and GC-MLP in EACN, NCP, and YRD during 2015-2024. Both bias-corrected models represent $PM_{2.5}$ changes attributable to anthropogenic emission changes relative to 2015.

For ozone, the role of emission changes also varies substantially across different periods and regions. During 2015-2019, emission changes cause widespread ozone increases across eastern China in both bias-

https://doi.org/10.5194/egusphere-2026-4864
Preprint. Discussion started: 31 August 2026

corrected models (Figs. 7c1 and d1). Over the NCP, emission-induced ozone increases reach 2.1 ppb year^{-1} in CMAQ-MLP and 1.7 ppb year^{-1} in GC-MLP, both substantially larger than the corresponding increases over the YRD (1.4 and 1.1 ppb year^{-1}, respectively). In contrast, during 2019-2024, both models suggest a substantially weakened increase or even a decrease in response to emission changes (Fig. 7c2 and d2). As discussed previously, NO_x emission reductions (18%) are more than twice as large as VOCs (8%) during 2015-2019, while their reduction rates become comparable (17% for NO_x and 13% for VOCs) during 2019-2023. Given the well-documented nonlinear response of ozone formation to its precursors, these shifts in NO_x and VOC emission trends are expected to significantly impact ozone concentrations.

We further examine ozone formation sensitivity over EACN using the satellite-derived formaldehyde-to-nitrogen dioxide ratio (FNR) (Fig. S3). Here, we apply empirical FNR thresholds reported in previous studies (Wang et al., 2021a) to classify ozone chemical formation regimes in China, with a focus on diagnosing their spatial contrasts and temporal shifts. During 2015-2019, VOC-limited conditions account for 52% of the NCP and 33% of the YRD, while transitional conditions account for 47% and 48%, respectively (Fig. S3). Under such high NO_x conditions, the rapid decrease in NO_x emissions is expected to elevate ozone concentrations, supported by many other modeling studies (Li et al., 2019a; Li et al., 2019b; Liu et al., 2023; Wang et al., 2019). In 2019-2024, continued NO_x emission reductions lead to a decreased proportion of VOC-limited conditions over the YRD (from 33% to 21%). The simultaneous decrease in NO_x and VOC emissions during this period may have become effective in slowing ozone increases or even reducing ozone over EACN, which explains the patterns shown in Figures 7c2 and d2.

In addition, emission-driven changes in $PM_{2.5}$ level further influence ozone by altering heterogeneous HO_2 uptake and photolysis (Li et al., 2019a). During 2015-2019, observed $PM_{2.5}$ decreases from 54.7 to 29.9 μg m^{-3} (-45%) over the NCP and from 35.5 to 23.4 μg m^{-3} (-34%) over the YRD, respectively. This rapid decline coincides with the positive emission-driven ozone response and may modulate it through weaker heterogeneous HO_2 uptake and enhanced photolysis (Gao et al., 2020; Li et al., 2019a; Liu and Wang, 2020b). From 2019 to 2024, $PM_{2.5}$ declines further to 22.6 μg m^{-3} over the NCP and 17.0 μg m^{-3} over the YRD, 24% and 27% below their 2019 levels. At these lower concentrations, previous studies suggest a weaker aerosol-mediated influence on ozone (Shao et al., 2021), which may partly explain the weaker emission-driven ozone response after 2019. This interaction highlights the value of coordinating continued $PM_{2.5}$ abatement with VOC and NO_x controls to achieve simultaneous reductions in $PM_{2.5}$ and ozone.

4.3 Meteorology-driven changes in $PM_{2.5}$ and ozone

Meteorological conditions strongly influence $PM_{2.5}$ and ozone variability through well-established physical and chemical processes (e.g., Fiore et al., 2012; Gong et al., 2022; Jacob and Winner, 2009; Tai et al., 2010). For $PM_{2.5}$, atmospheric ventilation and wet deposition are widely recognized as key meteorological processes governing aerosol accumulation and removal. The ventilation index, defined as the product of boundary layer height and wind speed, is an effective metric representing the atmospheric capacity for pollutant dispersion (e.g., Miao et al., 2019; Su et al., 2018; Sujatha et al., 2016; Sun et al., 2017), while precipitation is a usual variable indicating aerosol wet removal (Textor et al., 2006). Ventilation and precipitation are therefore examined below as the principal meteorological indicators for

https://doi.org/10.5194/egusphere-2026-4864
Preprint. Discussion started: 31 August 2026

interpreting the meteorology-driven $PM_{2.5}$ changes.

During 2015-2019, both CMAQ-MLP and GC-MLP consistently show that meteorological variabilities contribute to the $PM_{2.5}$ decline, although this contribution is much smaller and shows greater spatial variations than the dominant emission-driven decrease discussed in Sect. 4.2 (Fig. 9a1 and b1). The meteorology-driven $PM_{2.5}$ decline is larger over the NCP (-2.2 and -1.4 μg m^{-3} $year^{-1}$ in CMAQ-MLP and GC-MLP, respectively) compared with the YRD (-1.0 and -0.7 μg m^{-3} $year^{-1}$). This regional contrast is supported primarily by changes in atmospheric ventilation. The summertime ventilation index increases in both meteorological datasets, reaching 5-11% over the NCP and 4-8% over the YRD (Fig. 10d-f). The larger enhancement over the NCP indicates a stronger improvement in pollutant dispersion, consistent with the greater meteorology-driven $PM_{2.5}$ decrease in this region. Precipitation exerts a less uniform influence (Fig. 10a-c). WRF shows virtually no change in precipitation over the NCP and a small increase over the YRD (4%), suggesting that enhanced ventilation provides the principal meteorological signal associated with the CMAQ-MLP decreases. GEOS-FP, in contrast, shows a substantial precipitation increase over the NCP (46%) but a decrease over the YRD (-34%). Enhanced wet removal over the NCP therefore reinforces the improved ventilation, whereas reduced precipitation over the YRD partly offsets the effect of stronger ventilation.

Meteorological variabilities have a weaker effect on $PM_{2.5}$ during 2019-2024 compared with 2015-2019 (Figs. 9a2 and b2). CMAQ-MLP estimates a small meteorology-driven $PM_{2.5}$ increase across eastern China (0.2 μg m^{-3} $year^{-1}$), while GC-MLP indicates modest meteorology-driven $PM_{2.5}$ decreases (-0.8 μg m^{-3} $year^{-1}$), but again with notable spatial variations. The overall small meteorology-driven $PM_{2.5}$ change may reflect the competing effects of increased precipitation and weakened ventilation (Fig. 10a-f). Across WRF and GEOS-FP, precipitation increases by 34-92% over the NCP and 22-50% over the YRD, while the ventilation index decreases by 1-4% and 3-20%, respectively. However, accumulated precipitation is not a direct measure of wet scavenging, which also depends on rainfall frequency, intensity, duration, and aerosol properties (Hou et al., 2018; Wang et al., 2021c). These results also indicate that the MLP-corrected approach still has limitations in reconciling the attribution results from different models when multiple factors exert competing influences and the observed pollutant trend is relatively small.

https://doi.org/10.5194/egusphere-2026-4864
Preprint. Discussion started: 31 August 2026

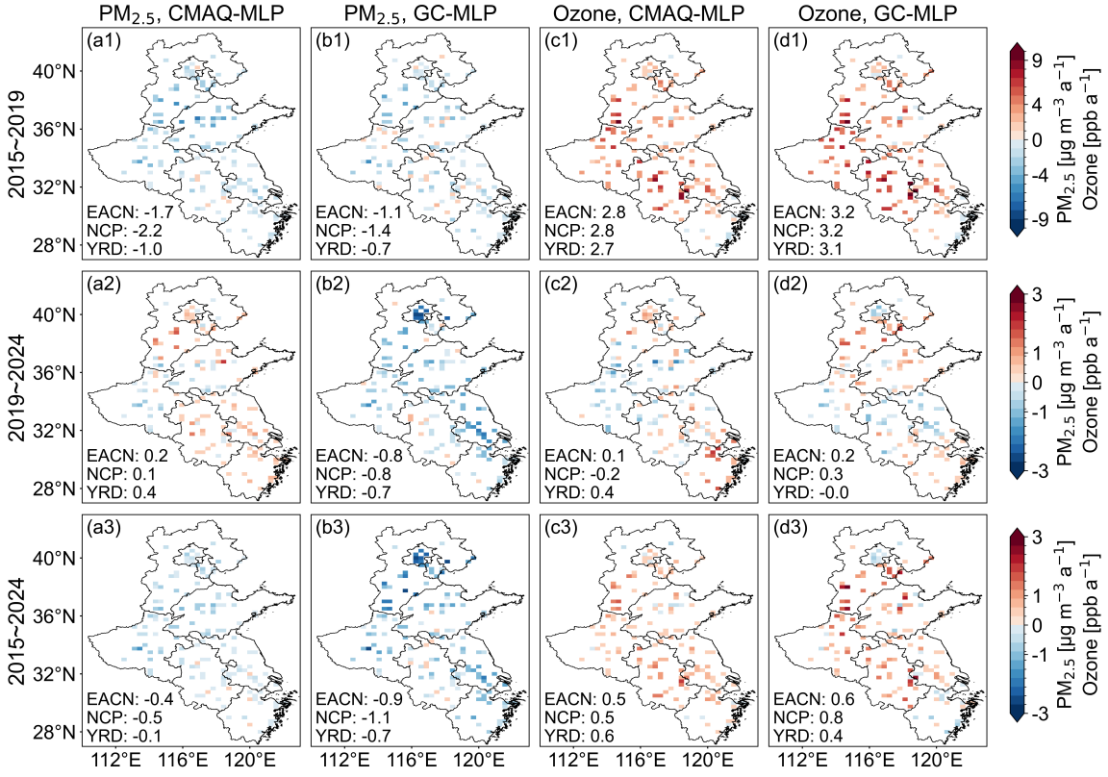

Figure 9. Same as Figure 7 but for meteorology-driven changes in daily $PM_{2.5}$ and MDA8 ozone.

570

https://doi.org/10.5194/egusphere-2026-4864
Preprint. Discussion started: 31 August 2026

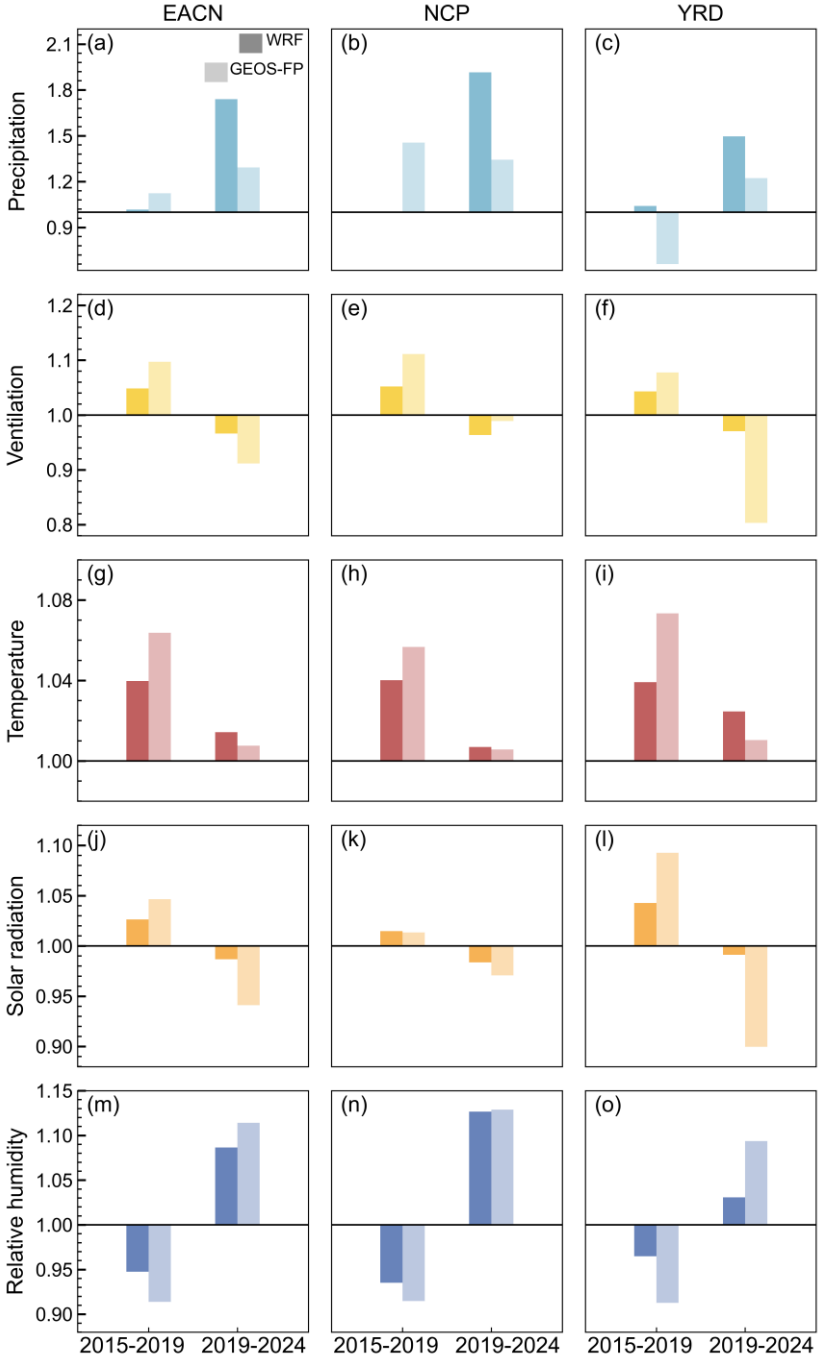

Figure 10. Relative changes in key meteorological variables across EACN, NCP, and YRD. Panels (a-c) present the relative changes in precipitation, panels (d-f) show ventilation, panels (g-i) show temperature, panels (j-l) show solar radiation, and panels (m-o) show relative humidity. Columns from left to right represent the three target regions. For the 2015-2019 period, relative changes represent values in 2019 relative to 2015. For the 2019-2024 period, relative changes represent values in 2024 relative to 2019. Within each panel, the darker and lighter shaded bars distinguish the meteorological fields derived from the WRF and GEOS-FP datasets, respectively.

https://doi.org/10.5194/egusphere-2026-4864
Preprint. Discussion started: 31 August 2026

Unlike $PM_{2.5}$, meteorological variabilities generally contribute to ozone increases over EACN in both models, although the magnitude differs between periods (Figs. 9c and d). We use summertime mean surface temperature, incoming shortwave radiation, and relative humidity to interpret these changes (Fig. 10g-o). Higher temperatures and stronger radiation accelerate photochemical reactions, while heat can also enhance biogenic emissions and suppress vegetation ozone uptake under drought conditions (Li et al., 2024b). Lower atmospheric moisture can suppress ozone loss (Chen et al., 2022; Li et al., 2025; Monks et al., 2015; Porter and Heald, 2019). These conditions are also typically associated with synoptic background such as atmospheric subsidence and stagnation, which favour ozone accumulation (Gao et al., 2021; Jiang et al., 2021; Yin et al., 2019). We therefore examine these variables to interpret the meteorology-driven ozone changes in this study.

During 2015-2019, meteorological variabilities consistently contribute to ozone increases over EACN in both bias-corrected models (Figs. 9c1 and d1). Regionally, the NCP and YRD show comparable meteorology-driven ozone increases of 2.8-3.2 and 2.7-3.1 ppb $year^{-1}$, respectively. Across WRF and GEOS-FP, temperature increases by 4-6% and 4-7%, radiation increases by 1-2% and 4-9%, and relative humidity decreases by 7-9% and 4-9% over the NCP and YRD, respectively (Fig. 10g-o). These shifts toward warmer, higher-radiation, and drier conditions support enhanced ozone formation in both regions. This relationship is particularly evident in 2019, when the meteorological variabilities increase ozone by 10.5 ppb in CMAQ-MLP and 12.3 ppb in GC-MLP over EACN relative to 2015 (Fig. 6b). This large meteorology-driven ozone anomaly is supported by the especially high surface temperature (up to 3 °C higher than the 2015 level), strong solar radiation, and the lowest relative humidity during 2015-2024 (Figs. S4 and S5). Consistent with our results, previous studies associate the exceptionally high ozone in 2019 with hot-drought conditions that weakened vegetation ozone uptake and dry deposition through drought-induced water stress (Lin et al., 2025) and with ozone-conducive circulation patterns. In particular, frequent northwesterly foehn flow promoted subsidence and warming, especially over the NCP (Li et al., 2020), while peripheral subsidence from multiple tropical cyclones and the persistent subtropical high dominated atmospheric conditions over eastern China (Hu et al., 2024). Both circulation patterns favoured ozone formation and accumulation.

During 2019-2024, meteorological variabilities only contribute to small ozone increases over EACN by 0.1 and 0.2 ppb $year^{-1}$ in CMAQ-MLP and GC-MLP, respectively (Figs. 9c2 and d2). We note that this small meteorology-driven ozone trend is masked by a sharp decrease from 2019 to 2020, followed by a modest increase in subsequent years (Fig. 6b). Regionally, meteorology-driven ozone changes are also small and are not consistent between the two models. We find that both the WRF and GEOS-FP meteorological data indicate a slight but much slower increase in surface temperature in this period (1%) compared with the 2015-2019 period (4-6%), and that increases in cloud cover and precipitation lead to a decline in solar radiation and an increase in relative humidity, neither of which is favourable for ozone photochemistry. The competing effects between increasing surface temperature and decreasing solar radiation may explain the small meteorological contribution to 2019-2024 ozone trend over EACN.

4.4 Comparison with existing studies and discussion

By correcting both CTMs and extending the study period through 2024, our analysis provides

https://doi.org/10.5194/egusphere-2026-4864
Preprint. Discussion started: 31 August 2026

improved, long-term quantifications of anthropogenic and meteorological contributions to the trends in both $PM_{2.5}$ and ozone. Consistent with previous studies focusing primarily on annual $PM_{2.5}$ changes or earlier study periods (e.g., before 2019) (Zhai et al., 2019; Zhang et al., 2019), our results focusing on summertime agree that anthropogenic emission reductions are the dominant driver of $PM_{2.5}$ decreases over eastern China. Specifically, our MLP-corrected results show that effective emission controls account for 63-94% of summertime $PM_{2.5}$ reductions during 2015-2019. In terms of ozone, previous studies have also suggested that summertime ozone increases during the early stage of China's clean air actions (e.g., 2013-2019) are driven by changes in anthropogenic emissions and are exacerbated by ozone-favourable weather conditions, although the relative contributions vary across these studies (e.g., Dang et al., 2021; Li et al., 2019a; Li et al., 2020; Liu and Wang, 2020a). Our results show that emission changes account for more than 50% of the ozone increase in both bias-corrected models in 2015-2019.

Extending the bias correction framework to 2024 reveals the evolving roles of anthropogenic emissions and meteorological variabilities in changes in both $PM_{2.5}$ and ozone. For $PM_{2.5}$, both CMAQ-MLP and GC-MLP show that emission reductions remain the dominant driver of the long-term decline during 2015-2024 (Fig. 11). However, the magnitude of emission-driven $PM_{2.5}$ decreases weakens during 2019-2024 despite continued declines in NO_2 and SO_2 concentrations. For ozone, both bias-corrected models reveal a shift in the effects of sustained precursor controls, from increasing ozone during 2015-2019 to near-neutral or weakly decreasing responses during 2019-2024. Meteorological variabilities contribute to substantial ozone increases during 2015-2019 but lead to weak ozone trends in 2019-2024. These findings extend previous shorter-period studies by showing that the effects of continued precursor controls on $PM_{2.5}$ and ozone evolve as pollution levels decline and atmospheric chemical regimes change.

Most existing studies apply a single CTM for attributing long-term trends in $PM_{2.5}$ or ozone to changes in anthropogenic emissions and meteorological conditions. A key limitation in this method is that CTMs struggle to reproduce observed trends even when driven by year-specific meteorological fields and anthropogenic emission inventories, which further bias the attribution and the interpretation of the relative role of emission and meteorology. In comparison, MLP-corrected simulations better reproduce observed pollutant levels, spatial distributions, and long-term trends (Sect. 3), and are therefore expected to provide a more accurate attribution. Here, we examine how model bias correction affects attribution estimates by comparing the attribution results from original CTMs and the MLP corrected results. For the CTM-only attribution, we use the results from the fixed-emission scenario for 2016-2024, in which anthropogenic emissions are held at their 2015 levels, to derive the meteorological contributions. The residual obtained by subtracting the CTM-derived meteorological trend from the observed pollutant trend is assigned to the emission-driven component. The original CTM-based spatial attribution results are shown in Figures S6 and S7 for comparison.

As summarized in Figure 11, the original CTM-based attribution results show large inter-model differences, especially for $PM_{2.5}$, whereas the MLP-corrected results yield more consistent contributions between CMAQ and GEOS-Chem. During 2015-2024, CMAQ attributes 94% of the $PM_{2.5}$ decline to emissions and 6% to meteorology, whereas GEOS-Chem shows that meteorological variabilities alone are sufficient to explain the observed $PM_{2.5}$ decline. This disagreement largely arises from their contrasting meteorological responses during 2019-2024. Over EACN, the meteorology-driven $PM_{2.5}$ trends are -5.3 $\mu g\ m^{-3}\ year^{-1}$ in GEOS-Chem and 0.1 $\mu g\ m^{-3}\ year^{-1}$ in CMAQ (Fig. S7), leaving residual emission-driven trends of 3.7 and -1.6 $\mu g\ m^{-3}\ year^{-1}$, respectively (Fig. S6). After correction, both models

https://doi.org/10.5194/egusphere-2026-4864
Preprint. Discussion started: 31 August 2026

identify emissions as the dominant $PM_{2.5}$ driver, contributing 69-83%, with meteorology contributing 17-31%. The MLP-corrected results also yield more consistent attribution for ozone (56-63% in MLP-corrected results vs 73-93% in original CTMs for emission contribution, respectively). The MLP correction reduces the inter-model attribution difference, defined as the absolute difference between the relative contributions estimated by the two models, from 136% to 14% for $PM_{2.5}$ and from 19% to 8% for ozone.

Attribution results derived from the original CTM-based approach here require accurate prediction of $PM_{2.5}$ and ozone in response to changes in meteorological conditions. However, this is one of the major challenges in current CTMs. Taking ozone response to temperature as an example, previous studies have shown that models underestimate the high summertime ozone-temperature sensitivity in China (Li and Lu, 2026; Wu et al., 2024), due to missing temperature-dependent anthropogenic emissions, such as enhanced power plant emissions of NO_x and evaporative anthropogenic VOCs (AVOCs) with temperatures, and land-atmosphere processes, such as vegetation physiological responses to drought stress through stomatal regulation (Lin et al., 2025). When such sensitivities are underestimated, CTM-only attributions of ozone variability tend to underestimate meteorological contribution, thereby assigning an artificially large contribution to emissions. By incorporating the MLP-predicted model biases, our framework better captures the sensitivity of ozone to meteorological factors such as temperature compared to traditional CTM methods, although improved statistical agreement does not necessarily imply better physical representation. Consistently, the MLP correction in our study increases the meteorological contribution from 8% to 37% in CMAQ and from 27% to 44% in GEOS-Chem. The MLP correction therefore reconciles pollutant- and model-specific sensitivities. Nevertheless, uncertainties remain because nonlinear emission-meteorology interactions, which are not isolated by fixed-emission simulations, are absorbed into the residual emission-driven contribution. Furthermore, the MLP model may be less reliable under chemical regimes or meteorological conditions unrepresented in the 2015-2019 training period.

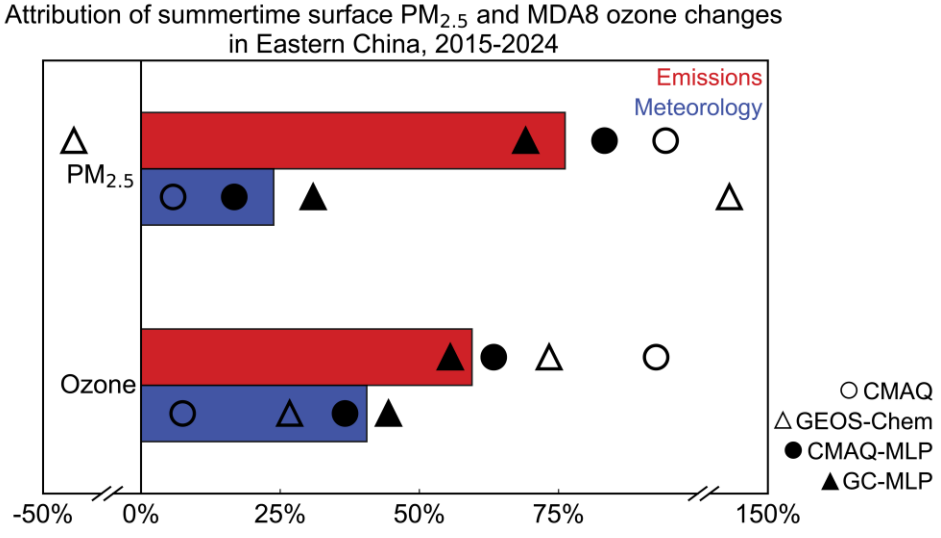

Figure 11. Comparison of emission and meteorological contributions to changes in $PM_{2.5}$ and MDA8 ozone concentrations during 2015-2024. Hollow symbols represent attribution results derived directly from the original chemical transport models (circles for CMAQ and

https://doi.org/10.5194/egusphere-2026-4864
Preprint. Discussion started: 31 August 2026

triangles for GEOS-Chem), whereas filled black symbols denote the corresponding attribution results after MLP bias correction (circles for CMAQ-MLP and triangles for GC-MLP). Horizontal bars indicate the mean of the two MLP-corrected attribution estimates, with red and blue bars representing contributions from anthropogenic emission changes and meteorological variabilities, respectively.

5 Conclusion

In this study, we develop a dual-CTM MLP bias correction framework to quantify the relative contributions of anthropogenic emissions and meteorological variabilities to summertime $PM_{2.5}$ and ozone changes over eastern China during 2015-2024. By integrating CMAQ and GEOS-Chem within a unified multi-pollutant framework, this approach provides observation-constrained attribution estimates for both pollutants, which enables attribution results to be evaluated across two structurally different models and allows robust attribution signals to be distinguished from model-dependent responses.

The MLP-corrected attribution results show that anthropogenic emission changes account for 69-83% of the long-term $PM_{2.5}$ decreases and 56-63% of the ozone changes during 2015-2024 across the two modeling frameworks. For $PM_{2.5}$, emission reductions remain the dominant driver throughout the study period, although the magnitude of emission-driven decreases weakens during 2019-2024 despite continued declines in observed precursor concentrations. The stronger $PM_{2.5}$ response over the ammonia-rich NCP than over the YRD further indicates that the effectiveness of precursor emission controls depends not only on the magnitude of emission reductions but also on regional atmospheric chemical environments. For ozone, the role of anthropogenic emissions evolves over time. Emission reductions promote ozone increases during 2015-2019 under predominantly VOC-limited conditions, but their effects weaken or shift toward suppressing ozone formation during 2019-2024 as ozone sensitivity moves away from strongly NO_x-saturated regimes. Meteorological variabilities, particularly warming and associated circulation conditions, continue to favour ozone formation and partially offset the benefits of emission reductions. These findings suggest that continued emission controls remain essential for air-quality improvement over eastern China. Future mitigation efforts may increasingly require integrated strategies that simultaneously address $PM_{2.5}$ and ozone, as the effectiveness of precursor emission reductions evolves under changing meteorological conditions, lower pollution levels, and shifting chemical regimes.

Methodologically, this study demonstrates the value of jointly constraining multiple pollutants and using multiple CTMs within a unified attribution framework. Correcting $PM_{2.5}$ and ozone together allows the model to account for their shared sensitivities to precursor emissions, atmospheric chemistry, and meteorological processes, rather than treating the two pollutants separately. Importantly, the MLP correction reduces the inter-model attribution difference from 136% to 14% for $PM_{2.5}$ and from 19% to 8% for ozone, thus mitigating the uncertainties inherent in standalone CTM attribution approaches. Applying the same observationally constrained procedure to CMAQ and GEOS-Chem further provides a way to evaluate whether attribution conclusions are consistent across different model structures. The framework therefore provides a practical approach for long-term multi-pollutant attribution in regions where CTMs retain valuable process information but exhibit systematic biases in simulated concentrations and trends. Nevertheless, this framework does not intrinsically modify the underlying physicochemical mechanisms within CTMs to more accurately simulate $PM_{2.5}$ and ozone concentrations

https://doi.org/10.5194/egusphere-2026-4864
Preprint. Discussion started: 31 August 2026

and their responses to emissions and meteorology. Moving forward, embedding machine learning directly into CTMs to correct these fundamental processes would be a highly beneficial next step.

Code and data availability

Hourly surface concentrations of air pollutants are archived at https://quotsoft.net/air (last access: 23 July 2026; Wang, 2026). The processed meteorological fields from GEOS-FP are available at http://geoschemdata.wustl.edu/ExtData/GEOS_0.25x0.3125/GEOS_FP/ (last access: 23 July 2026). The L3 OMI satellite data for NO_2 and HCHO are available at https://doi.org/10.5067/Aura/OMI/DATA3007 (last access: 23 July 2026; Krotkov et al., 2019) and https://doi.org/10.5067/Aura/OMI/DATA3010 (last access: 23 July 2026; Chance, 2019), respectively. The codes for machine learning algorithms used in this study can be accessed by contacting the corresponding author.

Author contributions

XL conceived the study and acquired funding supports. XL and XW designed the methodology and supervised the project. GZ conducted the WRF-CMAQ and GEOS-Chem simulations with significant help from HFW and HLW. GZ analysed the results, prepared the figures, and wrote the original draft, with substantial revision from XL and XW. All authors contributed to the interpretation of the results and revision of the manuscript.

Competing interests

Ke Li is a member of the editorial board of Atmospheric Chemistry and Physics. The authors have no other competing interests to declare.

Acknowledgements

We acknowledge funding support from National Key Research and Development Program of China (grant no. 2024YFC3714200), the National Natural Science Foundation of China (grant no. 42375092), and the Guangdong Basic and Applied Basic Research Foundation (grant nos. 2025B1515020034).

https://doi.org/10.5194/egusphere-2026-4864
Preprint. Discussion started: 31 August 2026

Financial support

This research has been supported by the National Key Research and Development Program of China (grant no. 2024YFC3714200), the National Natural Science Foundation of China (grant no. 42375092), and the Guangdong Basic and Applied Basic Research Foundation (grant nos. 2025B1515020034).

References

Bey, I., Jacob, D. J., Yantosca, R. M., Logan, J. A., Field, B. D., Fiore, A. M., Li, Q., Liu, H. Y., Mickley, L. J., and Schultz, M. G.: Global modeling of tropospheric chemistry with assimilated meteorology: Model description and evaluation, Journal of Geophysical Research: Atmospheres, 106, 23073-23095, https://doi.org/10.1029/2001jd000807, 2001.

Burnett, R., Chen, H., Szyszkowicz, M., Fann, N., Hubbell, B., Pope, C. A., 3rd, Apte, J. S., Brauer, M., Cohen, A., Weichenthal, S., Coggins, J., Di, Q., Brunekreef, B., Frostad, J., Lim, S. S., Kan, H., Walker, K. D., Thurston, G. D., Hayes, R. B., Lim, C. C., Turner, M. C., Jerrett, M., Krewski, D., Gapstur, S. M., Diver, W. R., Ostro, B., Goldberg, D., Crouse, D. L., Martin, R. V., Peters, P., Pinault, L., Tjepkema, M., van Donkelaar, A., Villeneuve, P. J., Miller, A. B., Yin, P., Zhou, M., Wang, L., Janssen, N. A. H., Marra, M., Atkinson, R. W., Tsang, H., Quoc Thach, T., Cannon, J. B., Allen, R. T., Hart, J. E., Laden, F., Cesaroni, G., Forastiere, F., Weinmayr, G., Jaensch, A., Nagel, G., Concin, H., and Spadaro, J. V.: Global estimates of mortality associated with long-term exposure to outdoor fine particulate matter, Proceedings of the National Academy of Sciences of the United States of America, 115, 9592-9597, https://doi.org/10.1073/pnas.1803222115, 2018.

Cao, J., Qiu, X., Liu, Y., Yan, X., Gao, J., and Peng, L.: Identifying the dominant driver of elevated surface ozone concentration in North China plain during summertime 2012-2017, Environmental Pollution, 300, 118912, https://doi.org/10.1016/j.envpol.2022.118912, 2022.

Chance, K.: OMI/Aura Formaldehyde (HCHO) Total Column Daily L3 Weighted Mean Global 0.1 degree Lat/Lon Grid V003, Goddard Earth Sciences Data and Information Services Center (GES DISC) [data set], accessed: 23 July 2026, https://doi.org/10.5067/Aura/OMI/DATA3010, 2019.

Chen, D., Liu, Z., Fast, J., and Ban, J.: Simulations of sulfate–nitrate–ammonium (SNA) aerosols during the extreme haze events over northern China in October 2014, Atmospheric Chemistry and Physics, 16, 10707-10724, https://doi.org/10.5194/acp-16-10707-2016, 2016.

Chen, L., Zhu, J., Liao, H., Yang, Y., and Yue, X.: Meteorological influences on PM2.5 and O3 trends and associated health burden since China's clean air actions, Science of The Total Environment, 744, https://doi.org/10.1016/j.scitotenv.2020.140837, 2020.

Chen, Q., Miao, R., Geng, G., Shrivastava, M., Dao, X., Xu, B., Sun, J., Zhang, X., Liu, M., Tang, G., Tang, Q., Hu, H., Huang, R.-J., Wang, H., Zheng, Y., Qin, Y., Guo, S., Hu, M., and Zhu, T.: Widespread 2013-2020 decreases and reduction challenges of organic aerosol in China, Nature Communications, 15, https://doi.org/10.1038/s41467-024-48902-0, 2024.

Chen, W., Wang, W., Jia, S., Mao, J., Yan, F., Zheng, L., Wu, Y., Zhang, X., Dong, Y., Kong, L., Zhong, B., Chang, M., Shao, M., and Wang, X.: A New Index Developed for Fast Diagnosis of Meteorological Roles in Ground-Level Ozone Variations, Advances in Atmospheric Sciences, 39, 403-414, https://doi.org/10.1007/s00376-021-1257-x, 2022.

Cohen, A. J., Brauer, M., Burnett, R., Anderson, H. R., Frostad, J., Estep, K., Balakrishnan, K., Brunekreef, B., Dandona, L., Dandona, R., Feigin, V., Freedman, G., Hubbell, B., Jobling, A., Kan, H., Knibbs, L., Liu, Y., Martin, R., Morawska, L., Pope, C. A., 3rd, Shin, H., Straif, K., Shaddick, G., Thomas, M., van Dingenen, R., van Donkelaar, A., Vos, T., Murray, C. J. L., and Forouzanfar, M. H.: Estimates and 25-year trends of the global burden of disease attributable to ambient air pollution: an analysis of data from the Global Burden of Diseases Study 2015, Lancet, 389, 1907-1918, https://doi.org/10.1016/S0140-6736(17)30505-6, 2017.

Dai, Q., Dai, T., Hou, L., Li, L., Bi, X., Zhang, Y., and Feng, Y.: Quantifying the impacts of emissions and meteorology on the interannual variations of air pollutants in major Chinese cities from 2015 to 2021, Science China Earth Sciences, 66, 1725-1737, https://doi.org/10.1007/s11430-022-1128-1, 2023.

https://doi.org/10.5194/egusphere-2026-4864
Preprint. Discussion started: 31 August 2026

Dang, R., Liao, H., and Fu, Y.: Quantifying the anthropogenic and meteorological influences on summertime surface ozone in China over 2012-2017, Science of The Total Environment, 754, 142394, https://doi.org/10.1016/j.scitotenv.2020.142394, 2021.

Dao, X., Wang, Z., Yuan, X., Li, W., Meng, X., Ma, G., Tong, E., and Zhang, F.: Spatiotemporal characteristics of PM2.5 components in the Beijing-Tianjin-Hebei region and its surrounding areas during the heating seasons from 2018 to 2023, Journal of Cleaner Production, 538, https://doi.org/10.1016/j.jclepro.2025.147210, 2026.

Fiore, A. M., Naik, V., Spracklen, D. V., Steiner, A., Unger, N., Prather, M., Bergmann, D., Cameron-Smith, P. J., Cionni, I., Collins, W. J., Dalsoren, S., Eyring, V., Folberth, G. A., Ginoux, P., Horowitz, L. W., Josse, B., Lamarque, J. F., MacKenzie, I. A., Nagashima, T., O'Connor, F. M., Righi, M., Rumbold, S. T., Shindell, D. T., Skeie, R. B., Sudo, K., Szopa, S., Takemura, T., and Zeng, G.: Global air quality and climate, Chemical Society Reviews, 41, 6663-6683, https://doi.org/10.1039/c2cs35095e, 2012.

Gao, C., Zhang, X. L., Xiu, A. J., Tong, Q. Q., Zhao, H. M., Zhang, S. C., Yang, G. Y., Zhang, M. D., and Xie, S. J.: Intercomparison of multiple two-way coupled meteorology and air quality models (WRF v4.1.1-CMAQ v5.3.1, WRF-Chem v4.1.1, and WRF v3.7.1-CHIMERE v2020r1) in eastern China, Geoscientific Model Development, 17, 2471-2492, https://doi.org/10.5194/gmd-17-2471-2024, 2024.

Gao, D., Xie, M., Liu, J., Wang, T., Ma, C., Bai, H., Chen, X., Li, M., Zhuang, B., and Li, S.: Ozone variability induced by synoptic weather patterns in warm seasons of 2014–2018 over the Yangtze River Delta region, China, Atmospheric Chemistry and Physics, 21, 5847-5864, https://doi.org/10.5194/acp-21-5847-2021, 2021.

Gao, J., Li, Y., Zhu, B., Hu, B., Wang, L., and Bao, F.: What have we missed when studying the impact of aerosols on surface ozone via changing photolysis rates?, Atmospheric Chemistry and Physics, 20, 10831-10844, https://doi.org/10.5194/acp-20-10831-2020, 2020.

Gardner, M. W. and Dorling, S. R.: Artificial neural networks (the multilayer perceptron)—a review of applications in the atmospheric sciences, Atmospheric Environment, 32, 2627-2636, https://doi.org/10.1016/S1352-2310(97)00447-0, 1998.

Geng, G., Zhang, Q., Tong, D., Li, M., Zheng, Y., Wang, S., and He, K.: Chemical composition of ambient PM2. 5 over China and relationship to precursor emissions during 2005–2012, Atmospheric Chemistry and Physics, 17, 9187-9203, https://doi.org/10.5194/acp-17-9187-2017, 2017.

Geng, G., Liu, Y., Liu, Y., Liu, S., Cheng, J., Yan, L., Wu, N., Hu, H., Tong, D., Zheng, B., Yin, Z., He, K., and Zhang, Q.: Efficacy of China's clean air actions to tackle PM2.5 pollution between 2013 and 2020, Nature Geoscience, 17, 987-994, https://doi.org/10.1038/s41561-024-01540-z, 2024.

Gong, S., Zhang, L., Liu, C., Lu, S., Pan, W., and Zhang, Y.: Multi-scale analysis of the impacts of meteorology and emissions on PM(2.5) and O(3) trends at various regions in China from 2013 to 2020 2. Key weather elements and emissions, Science of the Total Environment, 824, 153847, https://doi.org/10.1016/j.scitotenv.2022.153847, 2022.

Gu, B. J., Zhang, L., Van Dingenen, R., Vieno, M., Van Grinsven, H. J. M., Zhang, X. M., Zhang, S. H., Chen, Y. F., Wang, S. T., Ren, C. C., Rao, S., Holland, M., Winiwarter, W., Chen, D. L., Xu, J. M., and Sutton, M. A.: Abating ammonia is more cost-effective than nitrogen oxides for mitigating PM2.5 air pollution, Science, 374, 758-+, https://doi.org/10.1126/science.abf8623, 2021.

Guenther, A. B., Jiang, X., Heald, C. L., Sakulyanontvittaya, T., Duhl, T., Emmons, L. K., and Wang, X.: The Model of Emissions of Gases and Aerosols from Nature version 2.1 (MEGAN2.1): an extended and updated framework for modeling biogenic emissions, Geoscientific Model Development, 5, 1471-1492, https://doi.org/10.5194/gmd-5-1471-2012, 2012.

Hou, P., Wu, S., McCarty, J. L., and Gao, Y.: Sensitivity of atmospheric aerosol scavenging to precipitation intensity and frequency in the context of global climate change, Atmospheric Chemistry and Physics, 18, 8173-8182, https://doi.org/10.5194/acp-18-8173-2018, 2018.

Hou, T. Y., Yu, S. C., Jiang, Y. P., Chen, X., Zhang, Y. B., Li, M. Y., Li, Z., Song, Z., Li, P. F., Chen, J. M., and Zhang, X. Y.: Impacts of Chemical Initial Conditions in the WRF-CMAQ Model on the Ozone Forecasts in Eastern China, Aerosol and Air Quality Research, 22, https://doi.org/10.4209/aaqr.210402, 2022.

Hu, T., Lin, Y., Liu, R., Xu, Y., Ouyang, S., Wang, B., Zhang, Y., and Liu, S. C.: What caused large ozone variabilities in three megacity clusters in eastern China during 2015–2020?, Atmospheric Chemistry and Physics, 24, 1607-1626, https://doi.org/10.5194/acp-24-1607-2024, 2024.

Huang, X., Ding, A., Gao, J., Zheng, B., Zhou, D., Qi, X., Tang, R., Wang, J., Ren, C., Nie, W., Chi, X., Xu, Z., Chen, L., Li,

https://doi.org/10.5194/egusphere-2026-4864
Preprint. Discussion started: 31 August 2026

Y., Che, F., Pang, N., Wang, H., Tong, D., Qin, W., Cheng, W., Liu, W., Fu, Q., Liu, B., Chai, F., Davis, S. J., Zhang, Q., and He, K.: Enhanced secondary pollution offset reduction of primary emissions during COVID-19 lockdown in China, National Science Review, 8, nwaa137, https://doi.org/10.1093/nsr/nwaa137, 2021.

Hudman, R. C., Moore, N. E., Mebust, A. K., Martin, R. V., Russell, A. R., Valin, L. C., and Cohen, R. C.: Steps towards a mechanistic model of global soil nitric oxide emissions: implementation and space based-constraints, Atmospheric Chemistry and Physics, 12, 7779-7795, https://doi.org/10.5194/acp-12-7779-2012, 2012.

Jacob, D. J. and Winner, D. A.: Effect of climate change on air quality, Atmospheric Environment, 43, 51-63, https://doi.org/10.1016/j.atmosenv.2008.09.051, 2009.

Jiang, Y., Wang, S., Xing, J., Zhao, B., Li, S., Chang, X., Zhang, S., and Dong, Z.: Ambient fine particulate matter and ozone pollution in China: synergy in anthropogenic emissions and atmospheric processes, Environmental Research Letters, 17, https://doi.org/10.1088/1748-9326/aca16a, 2022.

Jiang, Z., Li, J., Lu, X., Gong, C., Zhang, L., and Liao, H.: Impact of western Pacific subtropical high on ozone pollution over eastern China, Atmospheric Chemistry and Physics, 21, 2601-2613, https://doi.org/10.5194/acp-21-2601-2021, 2021.

Keller, C. A., Evans, M. J., Knowland, K. E., Hasenkopf, C. A., Modekurty, S., Lucchesi, R. A., Oda, T., Franca, B. B., Mandarino, F. C., Díaz Suárez, M. V., Ryan, R. G., Fakes, L. H., and Pawson, S.: Global impact of COVID-19 restrictions on the surface concentrations of nitrogen dioxide and ozone, Atmospheric Chemistry and Physics, 21, 3555-3592, https://doi.org/10.5194/acp-21-3555-2021, 2021.

Krotkov, N. A., Lamsal, L. N., Marchenko, S. V., Celarier, E. A., Bucsela, E. J., Swartz, W. H., Joiner, J., and the OMI core team: OMI/Aura NO2 Cloud-Screened Total and Tropospheric Column L3 Global Gridded 0.25 degree × 0.25 degree V3, NASA Goddard Space Flight Center, Goddard Earth Sciences Data and Information Services Center (GES DISC) [data set], accessed: 23 July 2026, https://doi.org/10.5067/Aura/OMI/DATA3007, 2019.

Le, T. H., Wang, Y., Liu, L., Yang, J. N., Yung, Y. L., Li, G. H., and Seinfeld, J. H.: Unexpected air pollution with marked emission reductions during the COVID-19 outbreak in China, Science, 369, 702-+, https://doi.org/10.1126/science.abb7431, 2020.

LeCun, Y., Bengio, Y., and Hinton, G.: Deep learning, Nature, 521, 436-444, https://doi.org/10.1038/nature14539, 2015.

Li, D., Liu, H., and Wang, K.: Impacts of reductions in anthropogenic emissions from 2015 to 2024 on PM2.5 and meteorological conditions over China, Atmospheric Environment, 364, https://doi.org/10.1016/j.atmosenv.2025.121658, 2026.

Li, H., Zheng, B., Lei, Y., Hauglustaine, D., Chen, C., Lin, X., Zhang, Y., Zhang, Q., and He, K.: Trends and drivers of anthropogenic NO(x) emissions in China since 2020, Environmental Science and Ecotechnology, 21, 100425, https://doi.org/10.1016/j.ese.2024.100425, 2024a.

Li, K., Jacob, D. J., Liao, H., Shen, L., Zhang, Q., and Bates, K. H.: Anthropogenic drivers of 2013-2017 trends in summer surface ozone in China, Proceedings of the National Academy of Sciences of the United States of America, 116, 422-427, https://doi.org/10.1073/pnas.1812168116, 2019a.

Li, K., Jacob, D. J., Shen, L., Lu, X., De Smedt, I., and Liao, H.: Increases in surface ozone pollution in China from 2013 to 2019: anthropogenic and meteorological influences, Atmospheric Chemistry and Physics, 20, 11423-11433, https://doi.org/10.5194/acp-20-11423-2020, 2020.

Li, K., Jacob, D. J., Liao, H., Zhu, J., Shah, V., Shen, L., Bates, K. H., Zhang, Q., and Zhai, S.: A two-pollutant strategy for improving ozone and particulate air quality in China, Nature Geoscience, 12, 906-910, https://doi.org/10.1038/s41561-019-0464-x, 2019b.

Li, M., Huang, X., Yan, D., Lai, S., Zhang, Z., Zhu, L., Lu, Y., Jiang, X., Wang, N., Wang, T., Song, Y., and Ding, A.: Coping with the concurrent heatwaves and ozone extremes in China under a warming climate, Science Bulletin, 69, 2938-2947, https://doi.org/10.1016/j.scib.2024.05.034, 2024b.

Li, M., Kurokawa, J., Zhang, Q., Woo, J.-H., Morikawa, T., Chatani, S., Lu, Z., Song, Y., Geng, G., Hu, H., Kim, J., Cooper, O. R., and McDonald, B. C.: MIXv2: a long-term mosaic emission inventory for Asia (2010–2017), Atmospheric Chemistry and Physics, 24, 3925-3952, https://doi.org/10.5194/acp-24-3925-2024, 2024c.

Li, N., Zhang, H., Zhu, S., Liao, H., Hu, J., Tang, K., Feng, W., Zhang, R., Shi, C., Xu, H., Chen, L., and Li, J.: Secondary PM(2.5) dominates aerosol pollution in the Yangtze River Delta region: Environmental and health effects of the Clean air Plan, Environment International, 171, 107725, https://doi.org/10.1016/j.envint.2022.107725, 2023.

Li, S. and Lu, X.: Exploring the High Summertime Surface Ozone-Temperature Sensitivity in China, Environmental Science

& Technology, https://doi.org/10.1021/acs.est.6c04659, 2026.

Li, S., Wang, H., and Lu, X.: Anthropogenic emission controls reduce summertime ozone–temperature sensitivity in the United States, Atmospheric Chemistry and Physics, 25, 2725-2743, https://doi.org/10.5194/acp-25-2725-2025, 2025.

Lin, M. Y., Xie, Y. Y., De Smedt, I., and Horowitz, L. W.: Ozone Pollution Extremes in Southeast China Exacerbated by Reduced Uptake by Vegetation During Hot Droughts, Geophysical Research Letters, 52, https://doi.org/10.1029/2025GL114934, 2025.

Liu, J. and Xing, J.: Identifying Contributors to PM2.5 Simulation Biases of Chemical Transport Model Using Fully Connected Neural Networks, Journal of Advances in Modeling Earth Systems, 15, https://doi.org/10.1029/2021ms002898, 2023.

Liu, M., Huang, X., Song, Y., Xu, T., Wang, S., Wu, Z., Hu, M., Zhang, L., Zhang, Q., Pan, Y., Liu, X., and Zhu, T.: Rapid SO2 emission reductions significantly increase tropospheric ammonia concentrations over the North China Plain, Atmospheric Chemistry and Physics, 18, 17933-17943, https://doi.org/10.5194/acp-18-17933-2018, 2018.

Liu, Y. and Wang, T.: Worsening urban ozone pollution in China from 2013 to 2017 – Part 1: The complex and varying roles of meteorology, Atmospheric Chemistry and Physics, 20, 6305-6321, https://doi.org/10.5194/acp-20-6305-2020, 2020a.

Liu, Y. and Wang, T.: Worsening urban ozone pollution in China from 2013 to 2017 – Part 2: The effects of emission changes and implications for multi-pollutant control, Atmospheric Chemistry and Physics, 20, 6323-6337, https://doi.org/10.5194/acp-20-6323-2020, 2020b.

Liu, Y., Geng, G., Cheng, J., Liu, Y., Xiao, Q., Liu, L., Shi, Q., Tong, D., He, K., and Zhang, Q.: Drivers of Increasing Ozone during the Two Phases of Clean Air Actions in China 2013-2020, Environmental Science & Technology, 57, 8954-8964, https://doi.org/10.1021/acs.est.3c00054, 2023.

Lu, X., Zhang, L., Wang, X., Gao, M., Li, K., Zhang, Y., Yue, X., and Zhang, Y.: Rapid Increases in Warm-Season Surface Ozone and Resulting Health Impact in China Since 2013, Environmental Science & Technology Letters, 7, 240-247, https://doi.org/10.1021/acs.estlett.0c00171, 2020.

Lu, X., Hong, J., Zhang, L., Cooper, O. R., Schultz, M. G., Xu, X., Wang, T., Gao, M., Zhao, Y., and Zhang, Y.: Severe Surface Ozone Pollution in China: A Global Perspective, Environmental Science & Technology Letters, 5, 487-494, https://doi.org/10.1021/acs.estlett.8b00366, 2018.

Lu, X., Zhang, L., Chen, Y., Zhou, M., Zheng, B., Li, K., Liu, Y., Lin, J., Fu, T.-M., and Zhang, Q.: Exploring 2016–2017 surface ozone pollution over China: source contributions and meteorological influences, Atmospheric Chemistry and Physics, 19, 8339-8361, https://doi.org/10.5194/acp-19-8339-2019, 2019.

Lu, X., Ye, X., Zhou, M., Zhao, Y., Weng, H., Kong, H., Li, K., Gao, M., Zheng, B., Lin, J., Zhou, F., Zhang, Q., Wu, D., Zhang, L., and Zhang, Y.: The underappreciated role of agricultural soil nitrogen oxide emissions in ozone pollution regulation in North China, Nature Communications, 12, 5021, https://doi.org/10.1038/s41467-021-25147-9, 2021.

Lu, X., Liu, Y., Su, J., Weng, X., Ansari, T., Zhang, Y., He, G., Zhu, Y., Wang, H., Zeng, G., Li, J., He, C., Li, S., Amnuaylojaroen, T., Butler, T., Fan, Q., Fan, S., Forster, G. L., Gao, M., Hu, J., Kanaya, Y., Latif, M. T., Lu, K., Nédélec, P., Nowack, P., Sauvage, B., Xu, X., Zhang, L., Li, K., Koo, J.-H., and Nagashima, T.: Tropospheric ozone trends and attributions over East and Southeast Asia in 1995–2019: an integrated assessment using statistical methods, machine learning models, and multiple chemical transport models, Atmospheric Chemistry and Physics, 25, 7991-8028, https://doi.org/10.5194/acp-25-7991-2025, 2025.

Luecken, D. J., Yarwood, G., and Hutzell, W. T.: Multipollutant modeling of ozone, reactive nitrogen and HAPs across the continental US with CMAQ-CB6, Atmospheric Environment, 201, 62-72, https://doi.org/10.1016/j.atmosenv.2018.11.060, 2019.

McDuffie, E. E., Smith, S. J., O'Rourke, P., Tibrewal, K., Venkataraman, C., Marais, E. A., Zheng, B., Crippa, M., Brauer, M., and Martin, R. V.: A global anthropogenic emission inventory of atmospheric pollutants from sector- and fuel-specific sources (1970–2017): an application of the Community Emissions Data System (CEDS), Earth System Science Data, 12, 3413-3442, https://doi.org/10.5194/essd-12-3413-2020, 2020.

MEE: Ambient air quality standards (GB 3095-2026), https://www.mee.gov.cn/ywgz/fgbz/bz/bzwb/dqhjbh/dqhjzlbz/202602/t20260225_1144419.shtml (last access: 23 July 2026), 2026.

Miao, R., Chen, Q., Zheng, Y., Cheng, X., Sun, Y., Palmer, P. I., Shrivastava, M., Guo, J., Zhang, Q., Liu, Y., Tan, Z., Ma, X., Chen, S., Zeng, L., Lu, K., and Zhang, Y.: Model bias in simulating major chemical components of PM2.5 in China, Atmospheric Chemistry and Physics, 20, 12265-12284, https://doi.org/10.5194/acp-20-12265-2020, 2020.

https://doi.org/10.5194/egusphere-2026-4864
Preprint. Discussion started: 31 August 2026

Miao, Y., Li, J., Miao, S., Che, H., Wang, Y., Zhang, X., Zhu, R., and Liu, S.: Interaction Between Planetary Boundary Layer and PM2.5 Pollution in Megacities in China: a Review, Current Pollution Reports, 5, 261-271, https://doi.org/10.1007/s40726-019-00124-5, 2019.

Monks, P. S., Archibald, A. T., Colette, A., Cooper, O., Coyle, M., Derwent, R., Fowler, D., Granier, C., Law, K. S., Mills, G. E., Stevenson, D. S., Tarasova, O., Thouret, V., von Schneidemesser, E., Sommariva, R., Wild, O., and Williams, M. L.: Tropospheric ozone and its precursors from the urban to the global scale from air quality to short-lived climate forcer, Atmospheric Chemistry and Physics, 15, 8889-8973, https://doi.org/10.5194/acp-15-8889-2015, 2015.

Murray, L. T., Jacob, D. J., Logan, J. A., Hudman, R. C., and Koshak, W. J.: Optimized regional and interannual variability of lightning in a global chemical transport model constrained by LIS/OTD satellite data, Journal of Geophysical Research: Atmospheres, 117, https://doi.org/10.1029/2012JD017934, 2012.

Pinder, R. W., Adams, P. J., and Pandis, S. N.: Ammonia emission controls as a cost-effective strategy for reducing atmospheric particulate matter in the eastern United States, Environmental Science & Technology, 41, 380-386, https://doi.org/10.1021/es060379a, 2007.

Porter, W. C. and Heald, C. L.: The mechanisms and meteorological drivers of the summertime ozone–temperature relationship, Atmospheric Chemistry and Physics, 19, 13367-13381, https://doi.org/10.5194/acp-19-13367-2019, 2019.

Pye, H. O. T., Murphy, B. N., Xu, L., Ng, N. L., Carlton, A. G., Guo, H., Weber, R., Vasilakos, P., Appel, K. W., Budisulistiorini, S. H., Surratt, J. D., Nenes, A., Hu, W., Jimenez, J. L., Isaacman-VanWertz, G., Misztal, P. K., and Goldstein, A. H.: On the implications of aerosol liquid water and phase separation for organic aerosol mass, Atmospheric Chemistry and Physics, 17, 343-369, https://doi.org/10.5194/acp-17-343-2017, 2017.

Qu, K., Wang, X., Yan, Y., Jin, X., He, L.-Y., Huang, X.-F., Cai, X., Shen, J., Peng, Z., Xiao, T., Vrekoussis, M., Kanakidou, M., Brasseur, G. P., Daskalakis, N., Zeng, L., and Zhang, Y.: Unexpectedly persistent PM2.5 pollution in the Pearl River Delta, South China, in the 2015–2017 cold seasons: the dominant role of meteorological changes during the El Niño-to-La Niña transition over emission reduction, Atmospheric Chemistry and Physics, 25, 16983-17007, https://doi.org/10.5194/acp-25-16983-2025, 2025.

Shao, M., Wang, W., Yuan, B., Parrish, D. D., Li, X., Lu, K., Wu, L., Wang, X., Mo, Z., Yang, S., Peng, Y., Kuang, Y., Chen, W., Hu, M., Zeng, L., Su, H., Cheng, Y., Zheng, J., and Zhang, Y.: Quantifying the role of PM(2.5) dropping in variations of ground-level ozone: Inter-comparison between Beijing and Los Angeles, Science of The Total Environment, 788, 147712, https://doi.org/10.1016/j.scitotenv.2021.147712, 2021.

Shi, Z., Huang, L., Li, J., Ying, Q., Zhang, H., and Hu, J.: Sensitivity analysis of the surface ozone and fine particulate matter to meteorological parameters in China, Atmospheric Chemistry and Physics, 20, 13455-13466, https://doi.org/10.5194/acp-20-13455-2020, 2020.

Silver, B., Reddington, C. L., Chen, Y., and Arnold, S. R.: A decade of China's air quality monitoring data suggests health impacts are no longer declining, Environment International, 197, 109318, https://doi.org/10.1016/j.envint.2025.109318, 2025.

Sitch, S., Cox, P. M., Collins, W. J., and Huntingford, C.: Indirect radiative forcing of climate change through ozone effects on the land-carbon sink, Nature, 448, 791-794, https://doi.org/10.1038/nature06059, 2007.

Su, T., Li, Z., and Kahn, R.: Relationships between the planetary boundary layer height and surface pollutants derived from lidar observations over China: regional pattern and influencing factors, Atmospheric Chemistry and Physics, 18, 15921-15935, https://doi.org/10.5194/acp-18-15921-2018, 2018.

Sujatha, P., Mahalakshmi, D. V., Ramiz, A., Rao, P. V. N., Naidu, C. V., and Wang, Z.: Ventilation coefficient and boundary layer height impact on urban air quality, Cogent Environmental Science, 2, https://doi.org/10.1080/23311843.2015.1125284, 2016.

Sun, F., Cui, Y., Su, J., Shephard, M. W., Kharol, S. K., Zhang, Y., Shi, X., Zhang, J., Liu, H., Xiao, Q., Lu, X., Zeng, Z.-C., Griffis, T. J., and Hu, C.: Decadal changes in atmospheric ammonia and dry deposition across China inferred from space-ground measurements and model simulations, Atmospheric Chemistry and Physics, 25, 17907-17932, https://doi.org/10.5194/acp-25-17907-2025, 2025.

Sun, K., Liu, H., Wang, X., Peng, Z., and Xiong, Z.: The aerosol radiative effect on a severe haze episode in the Yangtze River Delta, Journal of Meteorological Research, 31, 865-873, https://doi.org/10.1007/s13351-017-7007-4, 2017.

Sun, R. Z., Lu, X., Lin, H. P., Wu, T. W., Ye, X. P., Shen, L., Wang, X., Wang, H. L., Li, J. Y., Lu, N., Su, J. Y., Zhang, J., Zhang, F., Xin, X. G., Liu, X., Yang, X., and Zhang, L.: Development of the global chemistry-climate coupled model

https://doi.org/10.5194/egusphere-2026-4864
Preprint. Discussion started: 31 August 2026

BCC-GEOS-Chem v2.0: improved atmospheric chemistry performance and new capability of chemistry-climate interactions, Geoscientific Model Development, 19, 2111-2136, https://doi.org/10.5194/gmd-19-2111-2026, 2026.

Tai, A. P. K., Mickley, L. J., and Jacob, D. J.: Correlations between fine particulate matter (PM2.5) and meteorological variables in the United States: Implications for the sensitivity of PM2.5 to climate change, Atmospheric Environment, 44, 3976-3984, https://doi.org/10.1016/j.atmosenv.2010.06.060, 2010.

Textor, C., Schulz, M., Guibert, S., Kinne, S., Balkanski, Y., Bauer, S., Berntsen, T., Berglen, T., Boucher, O., Chin, M., Dentener, F., Diehl, T., Easter, R., Feichter, H., Fillmore, D., Ghan, S., Ginoux, P., Gong, S., Grini, A., Hendricks, J., Horowitz, L., Huang, P., Isaksen, I., Iversen, I., Kloster, S., Koch, D., Kirkevåg, A., Kristjansson, J. E., Krol, M., Lauer, A., Lamarque, J. F., Liu, X., Montanaro, V., Myhre, G., Penner, J., Pitari, G., Reddy, S., Seland, Ø., Stier, P., Takemura, T., and Tie, X.: Analysis and quantification of the diversities of aerosol life cycles within AeroCom, Atmospheric Chemistry and Physics, 6, 1777-1813, https://doi.org/10.5194/acp-6-1777-2006, 2006.

Travis, K. R. and Jacob, D. J.: Systematic bias in evaluating chemical transport models with maximum daily 8 h average (MDA8) surface ozone for air quality applications: a case study with GEOS-Chem v9.02, Geoscientific Model Development, 12, 3641-3648, https://doi.org/10.5194/gmd-12-3641-2019, 2019.

Wang, H., Qiu, J., Liu, Y., Fan, Q., Lu, X., Zhang, Y., Wu, K., Shen, A., Xu, Y., Jin, Y., Zhu, Y., Sun, J., and Wang, H.: MEIAT-CMAQ: A modular emission inventory allocation tool for Community Multiscale Air Quality Model, Atmospheric Environment, 331, https://doi.org/10.1016/j.atmosenv.2024.120604, 2024a.

Wang, H., Lu, X., Palmer, P. I., Zhang, L., Lu, K., Li, K., Nagashima, T., Koo, J. H., Tanimoto, H., Wang, H., Gao, M., He, C., Wu, K., Fan, S., and Zhang, Y.: Deciphering decadal urban ozone trends from historical records since 1980, National Science Review, 11, nwae369, https://doi.org/10.1093/nsr/nwae369, 2024b.

Wang, H., Lu, X., Jacob, D. J., Cooper, O. R., Chang, K.-L., Li, K., Gao, M., Liu, Y., Sheng, B., Wu, K., Wu, T., Zhang, J., Sauvage, B., Nédélec, P., Blot, R., and Fan, S.: Global tropospheric ozone trends, attributions, and radiative impacts in 1995–2017: an integrated analysis using aircraft (IAGOS) observations, ozonesonde, and multi-decadal chemical model simulations, Atmospheric Chemistry and Physics, 22, 13753-13782, https://doi.org/10.5194/acp-22-13753-2022, 2022.

Wang, N., Lyu, X., Deng, X., Huang, X., Jiang, F., and Ding, A.: Aggravating O(3) pollution due to NO(x) emission control in eastern China, Science of The Total Environment, 677, 732-744, https://doi.org/10.1016/j.scitotenv.2019.04.388, 2019.

Wang, W., van der A, R., Ding, J., van Weele, M., and Cheng, T.: Spatial and temporal changes of the ozone sensitivity in China based on satellite and ground-based observations, Atmospheric Chemistry and Physics, 21, 7253-7269, https://doi.org/10.5194/acp-21-7253-2021, 2021a.

Wang, X., Fu, T. M., Zhang, L., Cao, H., Zhang, Q., Ma, H., Shen, L., Evans, M. J., Ivatt, P. D., Lu, X., Chen, Y., Zhang, L., Feng, X., Yang, X., Zhu, L., and Henze, D. K.: Sensitivities of Ozone Air Pollution in the Beijing-Tianjin-Hebei Area to Local and Upwind Precursor Emissions Using Adjoint Modeling, Environmental Science & Technology, 55, 5752-5762, https://doi.org/10.1021/acs.est.1c00131, 2021b.

Wang, X. L.: Historical air quality data in China, available at: https://quotsoft.net/air, last access: 23 July 2026.

Wang, Y., Xia, W., and Zhang, G. J.: What rainfall rates are most important to wet removal of different aerosol types?, Atmospheric Chemistry and Physics, 21, 16797-16816, https://doi.org/10.5194/acp-21-16797-2021, 2021c.

Wang, Y., Zhang, Q. Q., He, K., Zhang, Q., and Chai, L.: Sulfate-nitrate-ammonium aerosols over China: response to 2000–2015 emission changes of sulfur dioxide, nitrogen oxides, and ammonia, Atmospheric Chemistry and Physics, 13, 2635-2652, https://doi.org/10.5194/acp-13-2635-2013, 2013.

Weng, X., Forster, G. L., and Nowack, P.: A machine learning approach to quantify meteorological drivers of ozone pollution in China from 2015 to 2019, Atmospheric Chemistry and Physics, 22, 8385-8402, https://doi.org/10.5194/acp-22-8385-2022, 2022.

Weng, X., Li, J., Forster, G. L., and Nowack, P.: Large Modeling Uncertainty in Projecting Decadal Surface Ozone Changes Over City Clusters of China, Geophysical Research Letters, 50, https://doi.org/10.1029/2023gl103241, 2023.

Weng, X., Li, J., Zeng, G., Lu, X., Forster, G., and Nowack, P.: Divergent Ozone Predictions in China Under Carbon Neutrality: Why Chemical Mechanisms Disagree, Environmental Science & Technology, 60, 1977-1989, https://doi.org/10.1021/acs.est.5c10697, 2026.

WHO: WHO global air quality guidelines: particulate matter (PM2.5 and PM10), ozone, nitrogen dioxide, sulfur dioxide and carbon monoxide, World Health Organization, Geneva978-92-4-003422-8, 2021.

Wu, W., Fu, T. M., Arnold, S. R., Spracklen, D. V., Zhang, A., Tao, W., Wang, X., Hou, Y., Mo, J., Chen, J., Li, Y., Feng, X.,

https://doi.org/10.5194/egusphere-2026-4864
Preprint. Discussion started: 31 August 2026

Lin, H., Huang, Z., Zheng, J., Shen, H., Zhu, L., Wang, C., Ye, J., and Yang, X.: Temperature-Dependent Evaporative Anthropogenic VOC Emissions Significantly Exacerbate Regional Ozone Pollution, Environmental Science & Technology, 58, 5430-5441, https://doi.org/10.1021/acs.est.3c09122, 2024.

Xiao, Q., Geng, G., Xue, T., Liu, S., Cai, C., He, K., and Zhang, Q.: Tracking PM(2.5) and O(3) Pollution and the Related Health Burden in China 2013-2020, Environmental Science & Technology, 56, 6922-6932, https://doi.org/10.1021/acs.est.1c04548, 2022.

Xu, J.-W., Lin, J., Luo, G., Adeniran, J., and Kong, H.: Foreign emissions exacerbate PM2.5 pollution in China through nitrate chemistry, Atmospheric Chemistry and Physics, 23, 4149-4163, https://doi.org/10.5194/acp-23-4149-2023, 2023.

Yang, Y., Liao, H., and Lou, S.: Increase in winter haze over eastern China in recent decades: Roles of variations in meteorological parameters and anthropogenic emissions, Journal of Geophysical Research: Atmospheres, 121, https://doi.org/10.1002/2016jd025136, 2016.

Ye, X., Wang, X., and Zhang, L.: Diagnosing the Model Bias in Simulating Daily Surface Ozone Variability Using a Machine Learning Method: The Effects of Dry Deposition and Cloud Optical Depth, Environmental Science & Technology, 56, 16665-16675, https://doi.org/10.1021/acs.est.2c05712, 2022.

Ye, X., Zhang, L., Wang, X., Lu, N., Hickman, S., Luo, G., and Archibald, A. T.: Deciphering the impacts of meteorology on surface ozone variability in eastern China using explainable machine learning models, Atmospheric Chemistry and Physics, 26, 6377-6390, https://doi.org/10.5194/acp-26-6377-2026, 2026.

Yin, H., Lu, X., Sun, Y., Li, K., Gao, M., Zheng, B., and Liu, C.: Unprecedented decline in summertime surface ozone over eastern China in 2020 comparably attributable to anthropogenic emission reductions and meteorology, Environmental Research Letters, 16, https://doi.org/10.1088/1748-9326/ac3e22, 2021a.

Yin, H., Liu, C., Hu, Q., Liu, T., Wang, S., Gao, M., Xu, S., Zhang, C., and Su, W.: Opposite impact of emission reduction during the COVID-19 lockdown period on the surface concentrations of PM(2.5) and O(3) in Wuhan, China, Environmental Pollution, 289, 117899, https://doi.org/10.1016/j.envpol.2021.117899, 2021b.

Yin, Z., Cao, B., and Wang, H.: Dominant patterns of summer ozone pollution in eastern China and associated atmospheric circulations, Atmospheric Chemistry and Physics, 19, 13933-13943, https://doi.org/10.5194/acp-19-13933-2019, 2019.

Zhai, S., Jacob, D. J., Wang, X., Shen, L., Li, K., Zhang, Y., Gui, K., Zhao, T., and Liao, H.: Fine particulate matter (PM2.5) trends in China, 2013–2018: separating contributions from anthropogenic emissions and meteorology, Atmospheric Chemistry and Physics, 19, 11031-11041, https://doi.org/10.5194/acp-19-11031-2019, 2019.

Zhai, S., Jacob, D. J., Wang, X., Liu, Z., Wen, T., Shah, V., Li, K., Moch, J. M., Bates, K. H., Song, S., Shen, L., Zhang, Y., Luo, G., Yu, F., Sun, Y., Wang, L., Qi, M., Tao, J., Gui, K., Xu, H., Zhang, Q., Zhao, T., Wang, Y., Lee, H. C., Choi, H., and Liao, H.: Control of particulate nitrate air pollution in China, Nature Geoscience, 14, 389-395, https://doi.org/10.1038/s41561-021-00726-z, 2021.

Zhang, L., Chen, Y., Zhao, Y., Henze, D. K., Zhu, L., Song, Y., Paulot, F., Liu, X., Pan, Y., Lin, Y., and Huang, B.: Agricultural ammonia emissions in China: reconciling bottom-up and top-down estimates, Atmospheric Chemistry and Physics, 18, 339-355, https://doi.org/10.5194/acp-18-339-2018, 2018.

Zhang, Q., Streets, D. G., Carmichael, G. R., He, K. B., Huo, H., Kannari, A., Klimont, Z., Park, I. S., Reddy, S., Fu, J. S., Chen, D., Duan, L., Lei, Y., Wang, L. T., and Yao, Z. L.: Asian emissions in 2006 for the NASA INTEX-B mission, Atmospheric Chemistry and Physics, 9, 5131-5153, https://doi.org/10.5194/acp-9-5131-2009, 2009.

Zhang, Q., Zheng, Y., Tong, D., Shao, M., Wang, S., Zhang, Y., Xu, X., Wang, J., He, H., Liu, W., Ding, Y., Lei, Y., Li, J., Wang, Z., Zhang, X., Wang, Y., Cheng, J., Liu, Y., Shi, Q., Yan, L., Geng, G., Hong, C., Li, M., Liu, F., Zheng, B., Cao, J., Ding, A., Gao, J., Fu, Q., Huo, J., Liu, B., Liu, Z., Yang, F., He, K., and Hao, J.: Drivers of improved PM(2.5) air quality in China from 2013 to 2017, Proceedings of the National Academy of Sciences of the United States of America, 116, 24463-24469, https://doi.org/10.1073/pnas.1907956116, 2019.

Zhao, N., Zhang, Y., and Xue, L.: Nonlinear relationship between air pollution and precursor emissions in Qingdao, eastern China, Frontiers of Environmental Science & Engineering, 19, https://doi.org/10.1007/s11783-025-1929-3, 2024.

Zheng, B., Tong, D., Li, M., Liu, F., Hong, C., Geng, G., Li, H., Li, X., Peng, L., Qi, J., Yan, L., Zhang, Y., Zhao, H., Zheng, Y., He, K., and Zhang, Q.: Trends in China's anthropogenic emissions since 2010 as the consequence of clean air actions, Atmospheric Chemistry and Physics, 18, 14095-14111, https://doi.org/10.5194/acp-18-14095-2018, 2018.